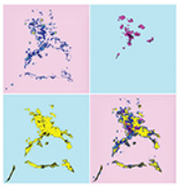
Autophagy



Autophagy

ISSN: 1554-8627 (Print) 1554-8635 (Online) Journal homepage: www.tandfonline.com/journals/kaup20

Loss of BECN1 does not compromise autophagosome formation but alters cargo selection and HLA-restricted antigen presentation of B cells

Svenja L. Walter , Felix Baur Lermer , Sophie Buchser , Sibilla Sander , Kennith Brian Castelino , Marcel Wacker , Eanna Fennell , Lisa Rieble , Saskia von Boxberg , Sandra Schmid , Christopher A. Hess , Laure-Anne Ligeon , Juliane Walz , Muriel Mari , Fulvio Reggiori , Jörn Dengjel & Christian Münz

To cite this article: Svenja L. Walter , Felix Baur Lermer , Sophie Buchser , Sibilla Sander , Kennith Brian Castelino , Marcel Wacker , Eanna Fennell , Lisa Rieble , Saskia von Boxberg , Sandra Schmid , Christopher A. Hess , Laure-Anne Ligeon , Juliane Walz , Muriel Mari , Fulvio Reggiori , Jörn Dengjel & Christian Münz (26 Aug 2026): Loss of BECN1 does not compromise autophagosome formation but alters cargo selection and HLA-restricted antigen presentation of B cells, Autophagy, DOI: 10.1080/15548627.2026.2719432

To link to this article: https://doi.org/10.1080/15548627.2026.2719432

© 2026 The Author(s). Published by Informa UK Limited, trading as Taylor & Francis Group.

View supplementary material

Published online: 26 Aug 2026.

Submit your article to this journal

Article views: 1074

View related articles

View Crossmark data

Full Terms & Conditions of access and use can be found at
https://www.tandfonline.com/action/journalInformation?journalCode=kaup20

AUTOPHAGY
https://doi.org/10.1080/15548627.2026.2719432

Taylor & Francis
by informa

RESEARCH PAPER

OPEN ACCESS Check for updates

Loss of BECN1 does not compromise autophagosome formation but alters cargo selection and HLA-restricted antigen presentation of B cells

Svenja L. Walter[a], Felix Baur Lermer[a], Sophie Buchser[b], Sibilla Sander[b], Kennith Brian Castelino[c], Marcel Wacker[d,e], Eanna Fennell[a,f], Lisa Rieble[a,g], Saskia von Boxberg[a], Sandra Schmid[a], Christopher A. Hess[a], Laure-Anne Ligeon[a], Juliane Walz[d,e,h,i], Muriel Mari [c], Fulvio Reggiori[c], Jörn Dengjel[b], and Christian Münz [a]

[a]Viral Immunobiology, Institute of Experimental Immunology, University of Zurich, Zurich, Switzerland; [b]Department of Biology, University of Fribourg, Fribourg, Switzerland; [c]Department of Biomedicine, University of Aarhus, Aarhus, Denmark; [d]Department of Peptide-Based Immunotherapy, Institute of Immunology, University and University Hospital Tübingen, Tübingen, Germany; [e]Cluster of Excellence iFIT (EXC2180) "Image-Guided and Functionally Instructed Tumor Therapies", University of Tübingen, Tübingen, Germany; [f]School of Medicine & Bernal Institute, University of Limerick, Limerick, Ireland; [g]Center of Infectious Medicine, Department of Medicine Huddinge, Karolinska Institutet, Huddinge, Sweden; [h]Clinical Collaboration Unit Translational Immunology, Department of Internal Medicine, University Hospital Tübingen, Tübingen, Germany; [i]German Cancer Consortium (DKTK), Partner Site Tübingen, A Partnership Between DKFZ and University Hospital Tübingen, Tübingen, Germany

ABSTRACT

BECN1 (beclin 1) is a member of the nucleation complex and considered crucial for induction of macroautophagy/autophagy, leading to the formation and ultimate degradation of autophagosomes. We found that in human B lymphoblastoid cell lines (LCLs) deficient of BECN1 (*BECN1*-KO), autophagosome formation was intact and autophagic flux could be induced upon nutrient starvation or MTOR inhibition. Remarkably, autophagosomal cargo differed significantly between *BECN1*-KO and control (CTRL) LCLs, revealing a preferred formation of autophagosomes at the endoplasmic reticulum (ER) and not at endosomes/lysosomes in *BECN1*-KO LCLs. Endosomal TLR3 (toll like receptor 3) was less frequently incorporated within autophagosomes in *BECN1*-KO LCLs. Additionally, several proteins of the ER-resident peptide loading complex for MHC class I antigen presentation were found enriched in autophagosomes from *BECN1*-KO LCLs, resulting in a diminished detection of *BECN1*-KO LCLs by T cells. Hence, BECN1 seems to be dispensable for autophagosome formation but rather contributes to cargo selection of phagophores and immunosurveillance.

ARTICLE HISTORY
Received 3 December 2025
Revised 10 August 2026
Accepted 12 August 2026

KEYWORDS
B cells; Beclin-1; CD8+ T cells; MHC class I; peptide loading complex

Abbreviations: ATG: autophagy-related; BECN1: beclin 1; CTRL: control; LCL: Epstein Barr virus transformed lymphoblastoid cell line; MHC: major histocompatibility complex; PLC: peptide-loading complex; TLR: toll like receptor.

INTRODUCTION

Macroautophagy, hereafter referred to as autophagy, is a conserved, catabolic process that promotes cell survival by recycling unused or damaged cellular components and is enhanced in response to nutrient deprivation. In brief, intracellular cargo is encapsulated within double-membraned vesicles termed autophagosomes that are transported to and fuse with lysosomes, resulting in the degradation of the enclosed lumen as well as the inner autophagosomal membrane [1].

During autophagy initiation, the ULK1-containing protein kinase complex associates with the endoplasmic reticulum (ER), driven by liquid-liquid phase separation, to establish the site of autophagosome biogenesis [2]. The BECN1 (beclin 1)-containing phosphatidylinositol 3-kinase (PtdIns3K) complex I is recruited subsequently to synthesize phosphatidylinositol-3-phosphate (PtdIns3P) at the forming phagophore, orchestrating the recruitment of downstream ATG (autophagy related) proteins through PI3P-binding proteins, such as WIPI2 (WD repeat domain, phosphoinositide interacting 2) [2]. The main autophagy marker MAP1LC3B/LC3B localizes to and accumulates on the forming autophagosomal membrane. Newly synthesized pro-LC3B is cleaved by ATG4B to expose a C-terminal glycine residue that can subsequently be targeted for phosphatidylethanolamine lipidation through a ubiquitin-like conjugation reaction involving ATG7, ATG3 and the ATG12–ATG5-ATG16L1 complex [1]. The processing of LC3B from its cytosolic form (LC3B-I) to its lipidated form (LC3B-II) is often used to test functional autophagy and monitor autophagic flux. Selective autophagy receptors, such as SQSTM1/p62, CALCOCO2/NDP52 and TAX1BP1 interact with membrane-bound LC3B-II as an anchor to recruit ubiquitinated proteins marked for degradation and are degraded along with their cargo once the closed autophagosome fuses with a lysosome.

CONTACT Christian Münz christian.muenz@uzh.ch Viral Immunobiology, Institute of Experimental Immunology, University of Zurich, Zurich, Switzerland
Supplemental data for this article can be accessed online at https://doi.org/10.1080/15548627.2026.2719432

© 2026 The Author(s). Published by Informa UK Limited, trading as Taylor & Francis Group.
This is an Open Access article distributed under the terms of the Creative Commons Attribution License (http://creativecommons.org/licenses/by/4.0/), which permits unrestricted use, distribution, and reproduction in any medium, provided the original work is properly cited. The terms on which this article has been published allow the posting of the Accepted Manuscript in a repository by the author(s) or with their consent.

BECN1 is considered crucial for the formation of classical autophagosomes as a core subunit of two PI3K complexes, functioning as a scaffold for its complex partners PIK3C3/VPS34, PIK3R4/VPS15, NRBF2, AMBRA1 and ATG14 or UVRAG [3]. The regulation of autophagy initiation is tightly linked to the availability and post-translational processing of BECN1. Sequestration of BECN1 by its high affinity binding partner BCL2 and other BCL2-protein family members prevents the formation of PI3K complexes, thus, inhibiting autophagy [4,5]. Additionally, autophagy-connected inducing and suppressing phosphorylations of BECN1 have been described, which mainly stabilize or disrupt the interactions of BECN1 with its complex partners [5]. Decreasing BECN1 protein levels or hindering of complex formation by BECN1 phosphorylation can inhibit autophagy and reduce autophagic flux upon starvation [6–8]. However, several studies have shown the existence of BECN1-independent autophagy, in which the loss of BECN1 has no effect on autophagy progression. These alternative pathways are still dependent on other core ATG proteins, such as ATG5 and ATG7, and can, in some instances, be induced by nutrient starvation [9–18]. Other evidence suggests that while BECN1 is dispensable for LC3B lipidation, it is still required for the functional formation of autophagosomes [19] or the localization of forming autophagosomes within the cytoplasm [20]. Although BECN1 has been extensively studied in the past, its exact function and role in autophagy appears to be highly cell type- or context-dependent.

Beyond its canonical role in cellular homeostasis and stress response, autophagy also contributes to immune regulation, including antigen processing and presentation. Recent studies have highlighted a selective form of autophagy that targets major histocompatibility complex class I (MHC-I) for degradation. In pancreatic ductal adenocarcinoma, NBR1-mediated autophagy facilitates degradation of ER-stalled MHC-I molecules through a multi-subunit capture complex [21,22]. Inhibition of ATG protein expression in this context results in increased MHC-I surface levels, enhancing $CD8^+$ T cell-mediated tumor responses. Similarly, immune related GTPase Q (IRGQ), a selective autophagy receptor, has been implicated in the degradation of MHC-I, affecting antigen presentation and $CD8^+$ T cell recognition in hepatocellular carcinoma [23]. Furthermore, MHC-I downregulation by the autophagic machinery has also been described for dendritic cells, dampening anti-viral $CD8^+$ T cell responses [24]. Despite this growing evidence linking autophagy to MHC-I degradation, the requirements for the core autophagy machinery, especially BECN1, in restricting MHC-I antigen presentation remains unexplored.

In this study, we show, that in human lymphoblastoid cell lines (LCLs), originating from B cell transformation by the human oncogenic Epstein Barr virus (EBV), loss of BECN1 does not influence LC3B lipidation or accumulation during starvation. Autophagosomes still form in the absence of BECN1 and starvation-induced autophagic flux can be detected in BECN1-deficient LCLs. However, the cargo sequestered within autophagosomes differs significantly in *BECN1*-KO compared to control (CTRL) LCLs. While endosomal and lysosomal proteins, such as toll-like receptor 3 (TLR3), were diminished in autophagosomes from BECN1-deficient LCLs, a significant enrichment of ER-resident proteins, such as the MHC-I peptide loading complex, was detected. Additionally, we show, that this has functional consequences by reducing MHC-I antigen presentation to $CD8^+$ T cells. Altogether, our results characterize a previously unrecognized role for BECN1 in determining autophagic cargo selectivity, thereby revealing a new link between autophagy and the regulation of antigen presentation.

RESULTS

Generation of LCL knockouts (KO) lacking BECN1, ATG4B or ATG5

Full knockout (KO) LCLs were generated using a CRISPR/Cas9 nucleofection approach with two guideRNAs, targeting the (+) and (-) DNA strand of the human *BECN1*, *ATG4B* or *ATG5* genes (Figure 1A). Control (CTRL) LCLs underwent the same procedure without guideRNA. Successful KO of *BECN1* was confirmed at the protein level by western blot using two distinct antibodies targeting amino acid residues 1–300 and 141–450, respectively (Figures 1B-C and 1H). Similarly, the absence of ATG4B or ATG5 proteins was validated and quantified by western blot (Figures 1D–1G). All three targeted proteins were undetectable in their respective KO LCLs, resulting in a significant reduction in protein levels upon quantification.

To assess the functional impact of the KOs, the LC3B-I to LC3B-II conversion was examined by western blot in LCLs treated with the lysosomal inhibitors bafilomycin A_1 (BafA1) or chloroquine (CQ) for three h (Figure 1I-L). In *ATG4B*- and *ATG5*-KO LCLs, only pro-LC3B and LC3B-I respectively, were detected, confirming the expected functional consequences of the gene KO. In *BECN1*-KO LCLs, however, LC3B-II formation and its accumulation in response to lysosomal inhibition remained comparable to CTRL LCLs, indicating that BECN1 deficiency does not substantially impair LC3B lipidation or turnover (Figures 1J and 1L).

To exclude the possibility that residual BECN1 expression might support autophagosome formation, KO validation was extended to mRNA and genomic levels. RT-qPCR using two different primer sets confirmed a strong depletion of full length *BECN1* mRNA, as well as in a shorter transcript representing approximately two-thirds of the full-length mRNA (Figure 1M). Sanger sequencing followed by ICE analysis (Synthego) demonstrated that, although only the C1 LCL might be clonal with both BECN1 copies mutated, no wild-type sequence remained in either LCL, further confirming complete KO of *BECN1* (Figure 1N). This suggested that ATG4B and ATG5 deficiency but not *BECN1*-KO compromises LC3 lipidation and autophagy progression in LCLs.

Autophagosomes form in BECN1-KO LCLs

To investigate whether the accumulation of LC3B-II in BECN1-deficient LCLs indicates intact autophagosome formation, immunofluorescent staining was performed after lysosomal inhibition with BafA1 or CQ for three h. Both treatments

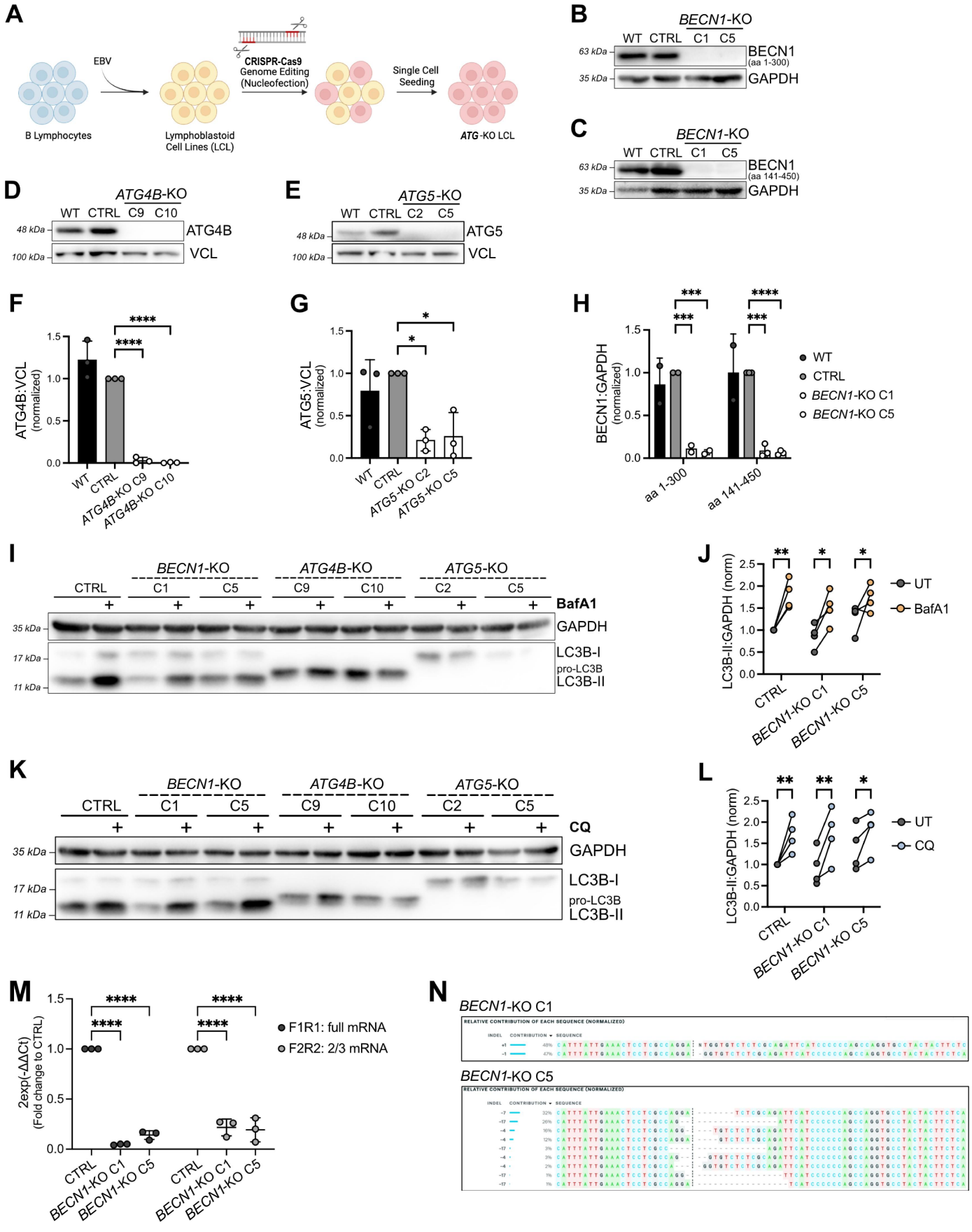


Figure 1. Validation of *ATG*-related gene knockouts (KO) in LCLs. (A) schematic strategy for the generation of KO LCLs. (B, C, H) loss of BECN1 was confirmed in LCLs after CRISPR-Cas9 targeting by western blot using two different antibodies, binding amino acids (aa) 1–300 and 141–450, respectively. Representative images (B, C) and quantification (H) are shown. GAPDH was used as the loading control. (D, E and F, G) *ATG4B* (D, F) and *ATG5* KO (E, G) deletion was confirmed and quantified by western blot. Representative images are shown. Vinculin (VCL) was used as loading control. (I-L) functional validation of the KOs was tested by LC3B western blot and

led to a significant increase of LC3 foci per cell in CTRL and both *BECN1*-KO LCLs (Figure 2A-B). As expected, LC3 did not form discernible foci in *ATG4B*- and *ATG5*-KO LCLs, confirming the expected functional consequences of these KOs (Figure 2B and S1A). To further strengthen the conclusion that the observed LC3 foci in CTRL and *BECN1*-KO LCLs represent autophagosomes, co-staining with the selective autophagy receptor (SAR) SQSTM1/p62 was performed. Treatment with BafA1 and CQ induced SQSTM1 accumulation and a significant increase in LC3 with SQSTM1 colocalizing foci in both, CTRL and BECN1-KO LCLs (Figure 2C-E and S1B). In contrast, *ATG4B*- and *ATG5*-KO LCLs displayed large SQSTM1 aggregates likely resulting from impaired degradation, without detectable LC3 foci or colocalization between LC3 and SQSTM1 (Figure 2D-E and S1A). Additionally, LC3 co-staining with a second SAR (CALCOCO2) revealed a similar pattern: CALCOCO2 foci accumulated and LC3 with CALCOCO2 colocalization increased upon BafA1 treatment in CTRL and *BECN1*-KO C1 (Figure 2F-G and S2). Notably, CALCOCO2 foci were less abundant in LCLs than SQSTM1 foci, with *BECN1*-KO LCL C5 showing minimal CALCOCO2 expression.

Finally, transmission electron microscopy (TEM) confirmed the presence of elongating phagophores and double-membraned autophagosomes and forming phagophores in *BECN1*-KO LCLs (Figure 3E). Importantly, no discernible differences were detected between autophagosomes from CTRL and *BECN1*-KO LCLs regarding size or morphology.

Taken together, these results demonstrate that autophagosomes form in BECN1-deficient LCLs and that selective cargo recruitment – via SQSTM1 and CALCOCO2 – remains functional.

Autophagic flux is inducible by nutrient starvation or MTOR inhibition in BECN1-KO LCLs

Since autophagosome formation appeared to be intact in *BECN1*-deficient LCLs, we next investigated autophagy induction and progression, using an additional approach to measure autophagic flux. For this purpose, a tandem fluorescence LC3 reporter (TFLC3) was used, with the GFP:RFP ratio measured by flow cytometry, which reflect autophagosome turnover due to GFP's sensitivity and RFP's relative resistance to lysosomal acidification (Figure 3A). Starvation drastically reduced the GFP signal, resulting in a decreased GFP:RFP ratio in both CTRL and *BECN1*-KO LCLs (Figure 3B-C). As anticipated, only minor changes were observed in *ATG4B*- and *ATG5*-KO LCLs upon starvation. Similarly, treatment with the MTOR (mechanistic target of rapamycin kinase) inhibitors torin-1 and rapamycin (Rapa) significantly decreased the GFP:RFP ratio in CTRL and *BECN1*-KO LCLs, while *ATG4B*- and *ATG5*-deficient LCLs remained largely unresponsive (Figure 3D and S3A). In line with established findings, co-treatment with BafA1 for one h slightly increased the GFP:RFP ratio in CTRL and *BECN1*-KO LCLs, reflecting an increase in lysosomal pH, resulting in diminished autophagic flux. Notably, while autophagy was inducible in *BECN1*-KO LCLs through starvation and direct MTOR inhibition, the response appeared to be slightly attenuated compared to CTRL LCLs. Nonetheless, the differences between treated CTRL and *BECN1*-KO LCLs were not statistically significant (Figure 3C-D). Moreover, diminished flux or changes in autophagosome degradation could not be detected as both, CTRL and *BECN1*-KO LCLs, showed similar LC3B-II accumulation dynamics after treatment with CQ for up to 48 h (Figure S3B-C) and lysosomal capabilities seem to be comparable as shown by LysoTracker staining with and without BafA1 treatment (Figure S3D). Additional experiments with two *BECN1*-KO clones from a second donor (D2; Figure S3E) confirmed LC3B-II accumulation in *BECN1*-deficient LCLs after lysosomal inhibition (Figure S3F-G), and autophagy flux was inducible through starvation in the absence of BECN1 (Figure S3H).

TEM confirmed the accumulation of autophagosomes and degradative compartments (DGC) in response to lysosomal inhibition in *BECN1*-KO LCLs, comparable to the effect observed in CTRL LCLs (Figure 3E-G). However, while autolysosomes appeared after co-treatment with torin-1 and BafA1 in *BECN1*-KO LCLs, these structures were less frequent than in similarly treated CTRL LCLs, also suggesting a reduction of autophagy flux (Figure 3H). Thus, *BECN1*-KO LCLs retain substantial autophagic flux that can be increased by starvation or MTOR inhibition.

Autophagosomal cargo differs significantly between BECN1-KO and CTRL LCLs

Since we were unable to detect significant changes of autophagic flux in the absence of BECN1, we hypothesized that autophagosomal cargo might be altered in *BECN1*-deficient LCLs. Accordingly, autophagosomes were purified from CTRL and *BECN1*-KO LCLs following a published protocol [25] and subsequently subjected to proteomic analysis by mass spectrometry (Figure 4A). The protocol was validated by western blot of the different cellular fractions and the subsequent LC3B co-immunoprecipitation (co-IP) from CTRL LCLs (Figure 4B). The presence of SQSTM1, CALCOCO2, SNAP29 and LC3A-II in the LC3B-IP sample confirmed the successful autophagosome purification. Pathway enrichment analysis using the STRING database [26] revealed significant differences in autophagosomal cargo between CTRL and *BECN1*-KO LCLs. While ER- and ribosome-associated proteins were strongly enriched in autophagosomes from *BECN1*-KO LCLs, lysosomal proteins were markedly reduced compared to CTRL LCLs (Figure 4D-E).

quantification after lysosomal inhibition using 100 nM BafA1 (I, J) or 50 µM CQ (K, L) for 3 h. Representative images are shown. (M) reduction of BECN1 full-length and shortened mRNA was detected by RT-qPCR. (N) genomic alterations resulting from CRISPR-Cas9 targeting on the *BECN1* genomic region were confirmed by sequencing and InDel analysis with synthego ICE in two different LCLs obtained from single cell seeding. F-H, J, L, M: statistical significance was determined using a one-way (F, G) or two-way (H, J, L, M) analysis of variance (ANOVA) followed by Bonferroni-corrected multiple comparison testing. Data represents the mean ± SD of at least 3 independent experiments. *$p \le 0.05$, **$p \le 0.01$, ***$p \le 0.001$, ****$p \le 0.0001$.

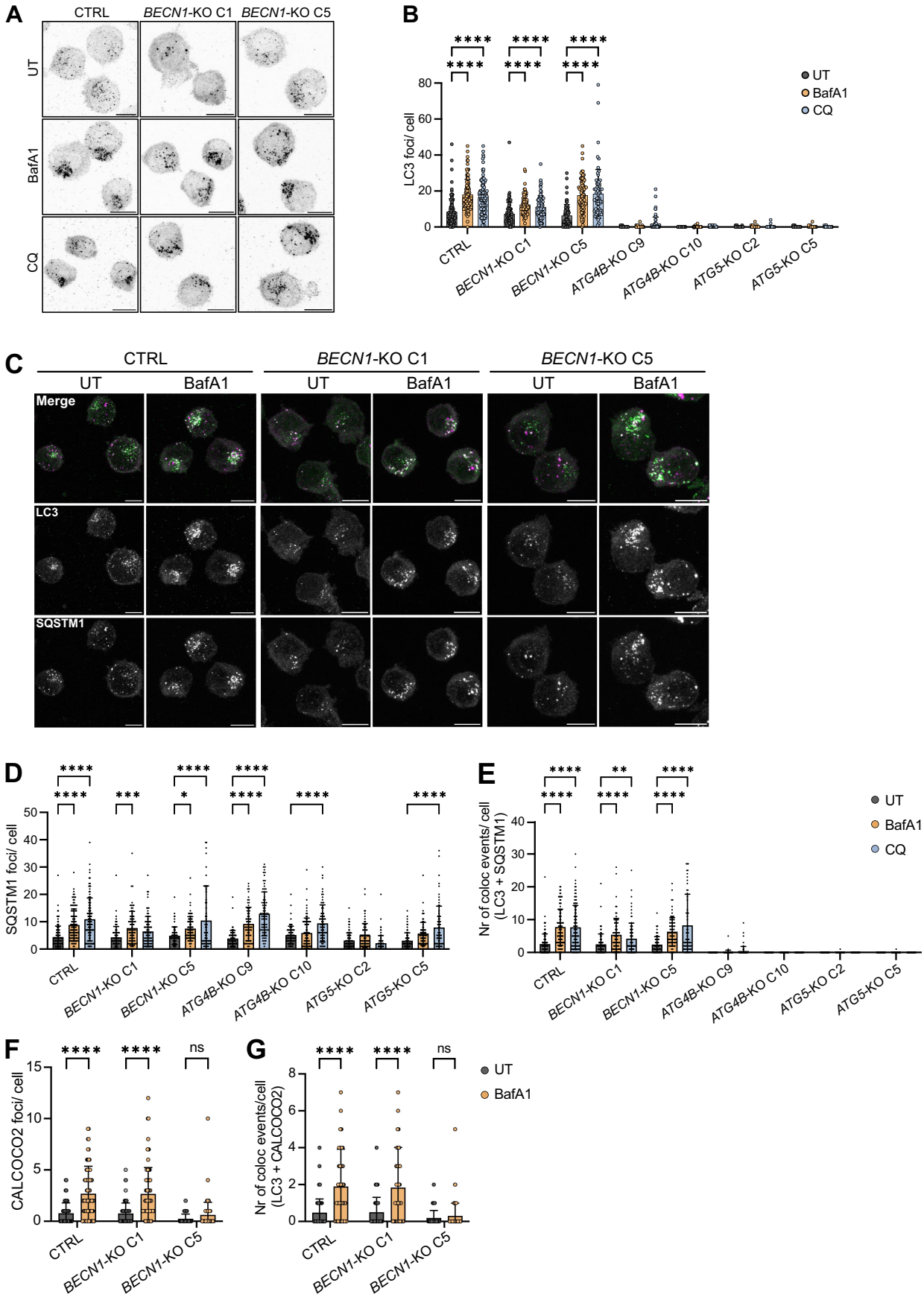


Figure 2. Autophagosomes form in *BECN1*-KO LCLs. (A, B) example images and quantification of the number of LC3 foci per cell by immunofluorescence staining in the specified LCLs after treatment with BafA1 (100 nM) or CQ (50 μM) for 3 h. Scale bars: 10 μm. (C) example images of LC3 (green) and SQSTM1/p62 (pink) foci in untreated and BafA1 (100 nM, 3 h) LCLs by immunofluorescence staining. Scale bars: 10 μm. (D, E) quantification of the number of SQSTM1/p62 foci (D) and the number of double positive SQSTM1/p62 with LC3 foci (E) per cell in LCLs after treatment with BafA1 (100 nM) or CQ (50 μM) for 3 h. (F, G) immunofluorescence

At the single protein level, several proteins involved in antigen processing and presentation – such as CALR (calreticulin), TAPBP/tapasin and PDIA3/ERp57 – were significantly enriched in *BECN1*-KO-derived autophagosomes (Figure 4C). Conversely, TLR3 was significantly reduced in *BECN1*-KO-derived LCLs autophagosomes (Figure 4C). Notably, while numerous mitochondrial proteins were detected as autophagosomal cargo in the mass spectrometry analysis, the majority of mitochondria-associated cargo did not show significant enrichment or reduction in *BECN1*-deficient LCLs in comparison to CTRL LCLs (Figure 4C).

These results demonstrate that loss of BECN1 alters autophagosomal cargo composition, leading to the selective enrichment of ER-resident proteins in autophagosomes and a reduction of ensodomal and lysosomal cargo.

TLR3 is significantly reduced in autophagosomes from BECN1-KO LCLs compared to CTRL LCLs

TLR3 was found reduced in *BECN1*-KO-derived autophagosomes with a particularly high fold change compared to autophagosomes purified from CTRL LCLs (FC = 4.2). TLR3 presence in autophagosomes was confirmed by western blot in purified autophagosomes from both CTRL and *BECN1*-KO LCLs (Figure 5A). The degradation of TLR3 appears to be partially dependent on autophagy, as lysosomal inhibition with BafA1 led to its accumulation in control LCLs after 6 and 24 h of treatment, but not at an earlier time point (three h) (Figure 5B-C and S4A-B). Notably, no TLR3 accumulation was observed in *BECN1*-KO LCLs at any time point, and TLR3 expression appeared to be generally reduced in whole cell lysates of *BECN1*-KO LCLs compared to CTRL LCLs (Figure 5B-C and S4A-B). Consistent with the mass spectrometry data, immunofluorescence staining revealed accumulation of TLR3 foci after three h of BafA1 treatment in CTRL LCLs but not in *BECN1*-KO LCLs (Figure 5D-E). Similarly, a significant increase in colocalization between TLR3 and LC3 could be detected, as shown in number of colocalizing foci (Figure 5F), and in percentage of colocalization only in CTRL LCLs (Figure S4D-E), reaching 20% of TLR3 colocalization with LC3 after 3 h of BafA1 treatment. The difference in BafA1 treatment time points observed between immunofluorescence and western blot data may be attributed to an earlier re-localization of TLR3 into foci detectable by immunofluorescence, while slow degradation dynamics are only evident in whole protein lysates at later time points.

To assess functional responsiveness to TLR3 stimulation, the well-characterized TLR3 agonist poly(I:C) was used. Overall, CTRL and *BECN1*-KO LCLs exhibited a comparable response to TLR3 stimulation, as measured by IL27 production and only slightly increased CXCL10 expression in BECN1-KO cells after stimulation (Figure 5G-H and S4G-J). As changes in IL27 and CXCL10 production after TLR3 stimulation were rather limited in both, CTRL and *BECN1*-KO LCLs, TLR3 signaling capacity might by inherently low in LCLs, and poly(I:C) failed to induce autophagic flux in CTRL and *BECN1*-KO LCLs (Figure S4F), despite previously reported autophagy inducing effects [27].

Generally, TLR3 appears to be expressed at low levels in B cells, as only a minute number of B cells showed detectable *TLR3* transcripts in two RNA-seq datasets of human B cells from the brains of humanized mice [28] and in three datasets of EBV-transformed B cells from patients [29] (data not shown). The few *TLR3* reads suggest minimal expression and would likely be excluded by standard RNA-seq filtering pipelines. Notably, *TLR3* mRNA seems to increase in B cells eight days post EBV infection (Log_2 FC = 2.5) [30], suggesting a potential association between EBV infection and the (transient) upregulation of TLR3. The only other TLR detected as autophagosomal cargo was TLR10, with no significant difference in its abundance between *BECN1*-KO and CTRL LCLs.

Together, these findings indicate that TLR3 is selectively degraded via basal autophagy in LCLs. BECN1 deficiency seems to impair this process, leading to altered TLR3 localization away from LC3. Given the relatively minor role of TLR3 signaling in B cells, this selective degradation does not produce pronounced functional effects, but it may have greater significance in other immune cell types.

Enrichment of MHC-I peptide loading complex (PLC) components in autophagosomes from BECN1-KO LCLs leads to reduced T cell recognition

Autophagosomes in *BECN1*-deficient LCLs seemed to preferentially target ER compared to those from CTRL LCLs. Several ER-resident proteins associated with the peptide loading complex (PLC) for MHC-I restricted antigen presentation, including CALR, TAPBP and PDIA3, were significantly enriched in *BECN1*-KO-derived autophagosomes (Figure 4C). All three proteins, along with CANX (calnexin), were detected at high levels in purified autophagosomes from both CTRL and *BECN1*-KO LCLs (Figure 6A-C). Interestingly, RNA-seq analysis by Mrozek-Gorska *et. al.* [30] revealed that CALR, CANX and PDIA3 are upregulated at various points during the first two weeks of EBV infection in B cells (Figure S5A).

To assess if increased autophagic degradation of the PLC would lead to reduced MHC-I trafficking to the cell membrane, citric acid mediated stripping was performed to remove MHC-I from the surface of treated cells, followed by monitoring of MHC-I recovery at various time points by flow cytometry. *BECN1*-deficient LCLs exhibited a delayed recovery of MHC-I across all measured time points, with a significant reduction observed at six h post-stripping (Figure 6D and

staining of LC3 and CALCOCO2 in LCLs: quantification of the number of CALCOCO2 foci (F) and double-positive LC3 with CALCOCO2 foci (G) per cell after treatment with BafA1 (100 nM) for 3 h. (B, D-G) statistical significance was determined by two-way ANOVA, followed by multiple comparison testing with Bonferroni correction. Data represents the mean ± SD of at 3 independent experiments. *$p \le 0.05$, **$p \le 0.01$, ***$p \le 0.001$, ****$p \le 0.0001$.

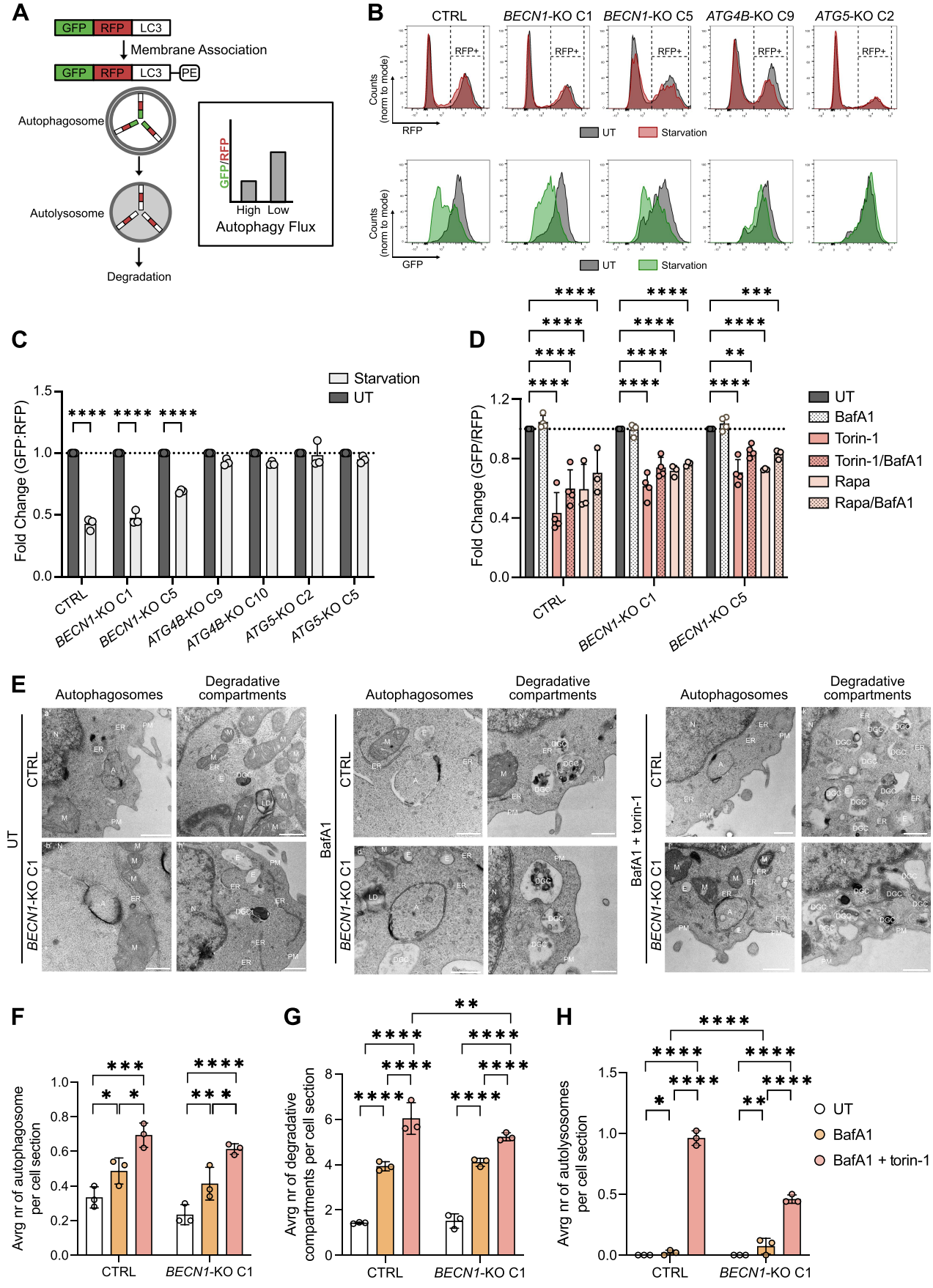


Figure 3. Autophagic flux is inducible by nutrient starvation or MTOR inhibition in *BECN1*-KO LCLs. (A) working principle of the tandem fluorescence reporter LC3 (TFLC3) construct used to measure autophagic flux. (B-D) RFP and GFP fluorescent signal was detected in TFLC3-expressing LCLs. (B) representative flow cytometry histograms are shown for RFP and GFP signal in untreated and starved (PBS, 24 h) LCLs. (C) quantification of the ratio of GFP to RFP geometric mean fluorescent intensity (MFI) in untreated and starved (PBS, 24 h) LCLs. Treated conditions were normalized to their respective untreated control (UT) (D) quantification of the ratio

S5B). The overall impaired recovery in *BECN1*-KO LCLs was further quantified by assessing the area under the curve (AUC) of the MHC-I surface recovery kinetics across all time points compared to CTRL LCLs (Figure 6E). Autophagy induction with torin-1 prior to citric acid strip markedly slowed MHC-I surface recovery in all LCLs, resulting in a one-third reduction of the AUC (Figure 6F-G and S5C), with *BECN1*-KO LCLs showing a trend toward even slower recovery compared to CTRL LCLs after induction. As previous studies have shown, MHC-I is degraded in an autophagy-dependent manner, resulting in reduced MHC-I surface levels [21,23,24]. We confirmed this observation in LCLs, as CTRL and *BECN1*-KO LCLs exhibited comparable surface levels of MHC-I, which was significantly reduced following autophagy induction by torin-1 (Figure 6H). However, BECN1 does not seem to play a crucial role during autophagy-dependent MHC-I degradation beyond targeting the PLC in B cells, as there were no significant differences detected in MHC-I surface levels between CTRL and *BECN1*-KO LCLs. Additionally, while HLA-A and HLA-C were detected in purified autophagosomes, no significant differences were found between CTRL and *BECN1*-KO LCLs (Figure 4C). The increased localization of PLC components to autophagosomes in *BECN1*-deficient LCLs could impair MHC-I folding and/or peptide loading in the ER. Such defects might lead to an increase of free class I heavy chain on the cell surface. Yet, CTRL and *BECN1*-KO LCLs showed similar baseline levels of free class I heavy chain, which were equally reduced after autophagy induction with torin-1, mirroring the reduction observed for fully assembled MHC-I (Figure S5D). Combined, these results suggest, that components of the PLC for MHC-I are sequestered within autophagosomes in general and – at least partially – degraded via autophagy in B cells, resulting in delayed MHC-I surface recovery upon autophagy initiation in all tested LCLs. The loss of BECN1 seems to enrich autophagosomal cargo with ER-resident proteins, including PLC components, resulting in slower MHC-I recovery in *BECN1*-KO LCLs even without autophagy induction, which may be further exacerbated upon autophagy activation.

To assess the functional consequences of altered MHC-I dynamics resulting from loss of BECN1, a transgenic, HLA-B35:01-restricted, EBNA1 (Epstein Barr virus nuclear antigen 1) $_{407–417}$-specific T cell receptor (TCR), based on the sequences of Cobo *et. al.* [31], was introduced into the Jurkat-Lucia^{TM} NFAT reporter cell line (Figure 6I) via lentiviral transduction. The respective lentivirus encoded the recombinant TCR containing human variable TCRα and β chain domains, mouse constant TCRα and β chain domains to avoid mispairing with the endogenous human TCR, and a truncated CD19 sequence to assess transduction efficiency. Successful transduction was confirmed by flow cytometry, staining for murine CD19 and the murine TCR β chain (Figure 6J). Upon co-culture with LCLs pulsed with the cognate peptide, the TCR-transduced Jurkat-Lucia^{TM} cells exhibited significantly reduced activation when incubated with *BECN1*-deficient LCLs, compared to CTRL LCLs (Figure 6K). Notably, treatment with torin-1 did not change the ability of both LCLs, CTRL and *BECN1*-KO, to induce activation of the reporter cell line. Moreover, a trend to reduced T cell activation by *BECN1*-deficient LCLs was observed even with unpulsed LCLs (Figure S5E). Autophagy inhibition with a PIK3C3/VPS34 inhibitor or Wortmannin increased T cell recognition, indicating that functional autophagy indeed limits T cell recognition through MHC-I in this setting (Figure S5F). Functional differences were further examined in a more physiological context using primary human CD3$^+$ T cells. Transduction efficacy of the transgenic TCR was assessed by flow cytometry (Figure 6L) prior to co-culture with peptide-pulsed LCLs. In line with the results described above, primary T cells showed a reduced activation when co-cultured with *BECN1*-deficient LCLs as shown by a lower expression of activation markers CD69 and 4–1BB on CD8$^+$ T cells (Figure 6M and S5G) and reduced production of IFNG/IFN β (Figure 6N and S5H). Notably, reduced T cell recognition of *BECN1*-KO LCLs was more pronounced with TCR transduced primary T cells than with the Jurkat-Lucia reporter cells. In order to identify the BECN1 domain that can restore T cell recognition, a transcomplementation assay was performed, using lentiviral transduction to introduce transgenic wild-type BECN1 or the BECN1^{R139A} mutant, incapable of binding BCL2, into *BECN1*-KO LCLs (Figure S5I). Co-culture with Jurkat-Lucia^{TM} cells showed a clear trend toward increased recognition after transcomplementation with both BECN1 variants in CTRL and BECN1-KO LCLs (Figure S5J), suggesting that excess BECN1 generally aids T cell recognition in LCLs and that BCL2 binding is dispensable for this function.

In conclusion, *BECN1*-KO LCLs are less efficiently recognized by T cells and show reduced capabilities to activate them. This effect is not due to lower MHC-I surface levels (Figure 6H) or a drastic defect in MHC-I assembly, which would otherwise lead to an increase in free class I heavy chains (Figure S5B), but seem to result from less efficient peptide loading after preferential targeting of the PLC by autophagy.

Additionally, half-life of peptide-MHC-I complexes on the cell surface does not appear to be substantially affected by loss of BECN1. Both CTRL and *BECN1*-KO LCLs that were washed and rested for 3 h after peptide-pulsing prior to co-

of GFP to RFP MFI in LCLs treated either with torin-1 (100 nM) or rapamycin (Rapa) [20 nM] for 24 h alone or in combination with BafA1 (100 nM) for one hour. Treated conditions were normalized to their respective untreated control (UT). (E) TEM images of autophagosomes (a-f) and degradative compartments (g-l) in CTRL and *BECN1*-KO C1 LCLs. Cells were either untreated or treated with BafA1 (100 nM) for 3 h alone or in combination with torin-1 -(100 nM) for 24 h. A = autophagosome, DGC = degradative compartment, E = endosome, ER = endoplasmic reticulum, G = golgi apparatus, LD = lipid droplet, *M* = mitochondria, *N* = nucleus, PM = plasma membrane. Scale bars: 500 nm. (F-H) quantification of TEM images, counting autophagosomes (F), degradative compartments (G) and autolysosomes (H). (C, D) statistical significance was determined with a two-way ANOVA, followed by multiple comparison testing with Bonferroni or Tukey correction. Data represents the mean ± SD of at least 3 independent experiments. (F-H) statistical significance was evaluated using the two-tailed heteroscedastic t-test. Data represents 150 random cell sections from three independent grids. *$p \le 0.05$, **$p \le 0.01$, ***$p \le 0.001$, ****$p \le 0.0001$.

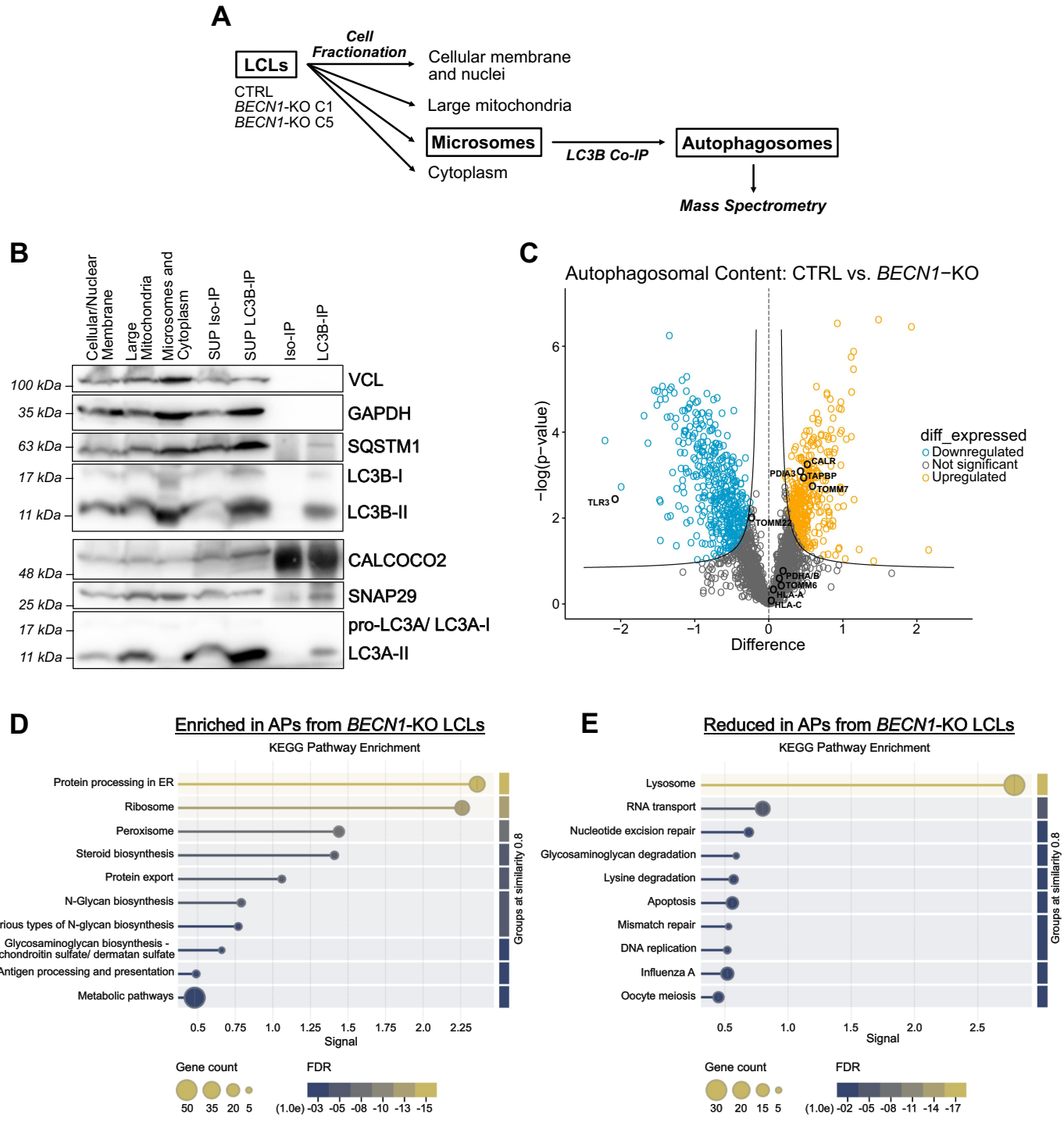


Figure 4. Autophagosomal cargo differs significantly between *BECN1*-KO and CTRL LCLs. (A) autophagosomes were purified from CTRL and *BECN1*-KO LCLs by cell fractionation, followed by LC3B co-IP and analyzed by mass spectrometry. (B) autophagosome purification was validated in CTRL LCLs by western blot of the cellular fractions and IP samples. Cellular control proteins (GAPDH, VCL [vinculin]) as well as known autophagy markers and cargo receptors (LC3B, LC3A, SQSTM1, CALCOCO2 and SNAP29) were tested. Representative images are shown. (C) differential abundance analysis of enriched and reduced proteins, comparing both *BECN1*-KO LCLs together to CTRL LCLs. Mass spectrometry intensities of proteins were log2-transformed, median-normalized and isotype-controlled beforehand. Statistical significance was determined by a two-sided t-test with multiple testing correction using a permutation-based false-discovery rate (250 randomizations, FDR = 0.05). (D, E) pathway enrichment analysis of peptides found in autophagosomes from *BECN1*-KO LCLs compared to CTRL LCLs, using the STRING database [26]. Shown are KEGG pathway annotations of significantly enriched (D) and reduced (E) pathways (grouped by similarity ≥ 0.8, minimal signal shown ≥ 0.01, minimal strength shown ≥ 0.01, maximum FDR shown ≤ 0.05).

culture with Jurkat-Lucia™ cells were recognized as efficiently as LCLs which had been continuously incubated with the cognate peptide (Figure S5K). Similarly, no major defects in MHC-I internalization were observed in *BECN1*-deficient LCLs. CTRL and *BECN1*-KO LCLs both showed a clear decrease in antibody labeled surface MHC-I signal relative to cytoplasmic signal after 1.5 and 3 h of internalization (Figure S6A-B).

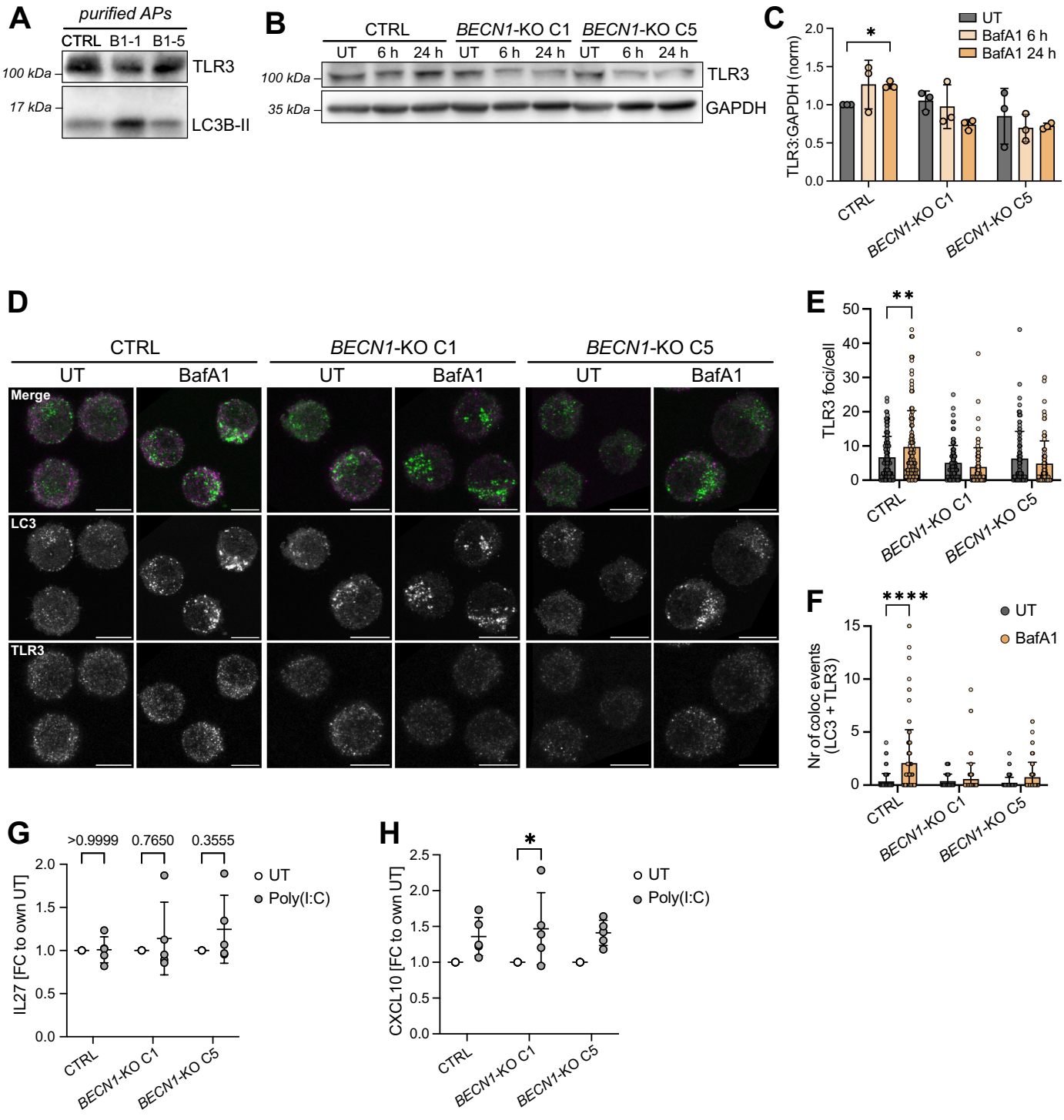


Figure 5. TLR3 is significantly reduced in autophagosomes from *BECN1*-KO LCLs compared to CTRL LCLs. (A) western blot detection of TLR3 in purified autophagosomes. Representative images are shown. (B, C) Representative images (B) and quantification (C) of TLR3 accumulation in indicated LCLs after treatment with BafA1 (100 nM) for 6 or 24 h. (D) example images of LC3 (green) and TLR3 (pink) foci in untreated and BafA1 (100 nM, 3 h) treated LCLs by immunofluorescence staining. (E, F) quantification of the number of TLR3 foci (E) and the number of double-positive TLR3-LC3 foci (F) per cell in indicated LCLs after treatment with BafA1 (100 nM) for 3 h. Representative images are shown. Scale bars: 10 µm. (G, H) detection of IL27 (G) and CXCL10 (H) in the supernatant of CTRL and BECN1-KO LCLs after poly(I:C) treatment (25 µg/mL) for 24 h. (C, E, F, G-H) statistical significance was determined by two-way ANOVA, followed by multiple comparison testing with Bonferroni or Sidak correction. Data represents the mean ± SD of at least 3 independent experiments. *$p \leq 0.05$, **$p \leq 0.01$, ****$p \leq 0.0001$.

Finally, we also assessed the MHC-I ligand composition after immune affinity purification of MHC-I complexes and peptide elution followed by mass spectrometry (Figure S6C, displayed as a Venn diagram [32]). While only few MHC ligands could be identified that where filtered to match the peptide binding motifs of the HLA class I haplotype of our

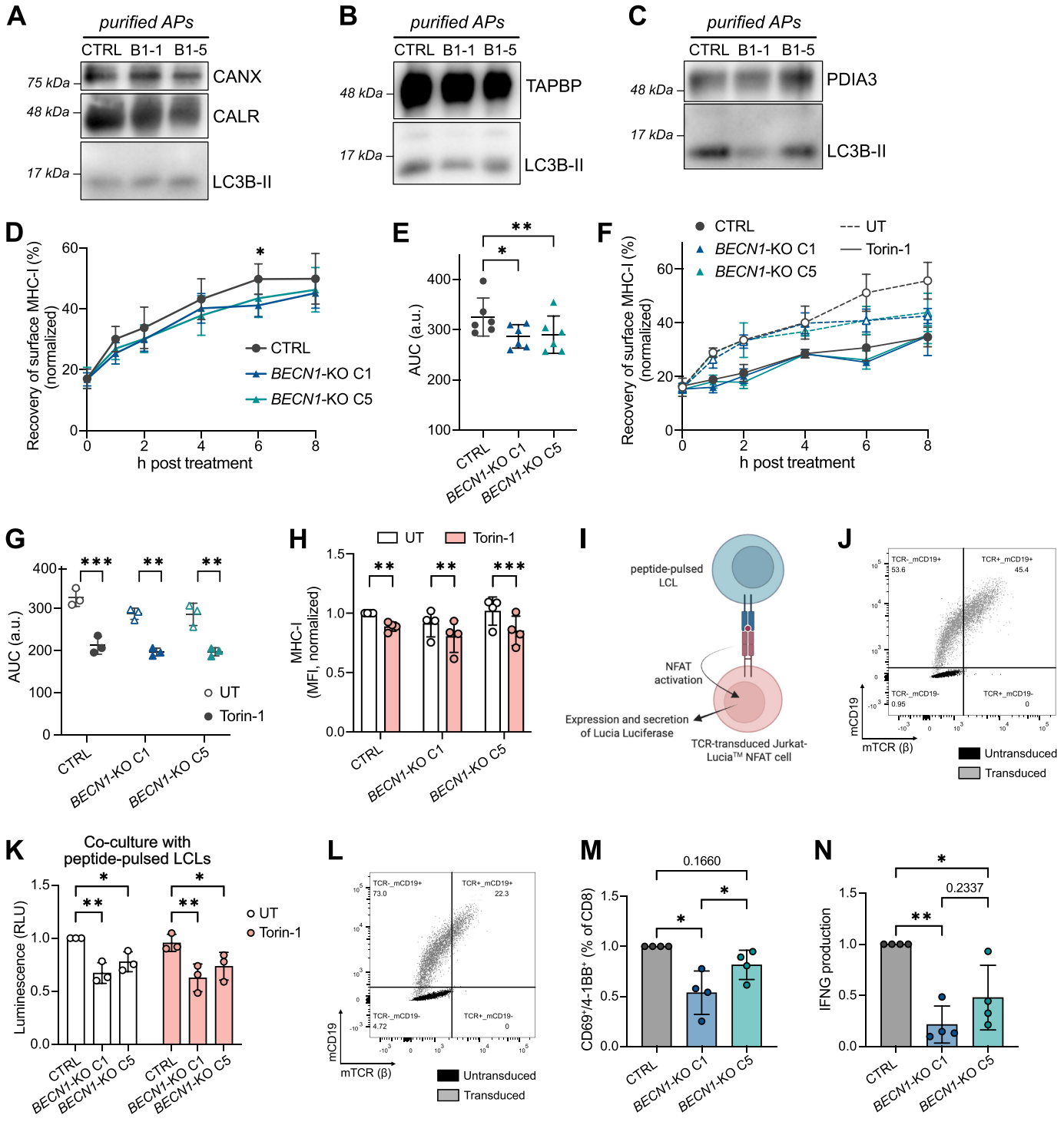


Figure 6. Enrichment of PLC components in autophagosomes from *BECN1*-KO LCLs leads to reduced T cell recognition. (A, B, C) western blot detection of CANX and CALR (A), TAPBP (B) and PDIA3 (C) in purified autophagosomes. Representative images are shown. (D) recovery of surface MHC-I on the surface of LCLs after stripping with citric acid. Percentage of recovery was determined by flow cytometry. Recovery was normalized to the respective untreated sample. (E) quantification of the area under the curve (AUC) of the recovery of surface MHC-I shown in D. (F) LCLs were treated with torin-1 (100 nM) for 24 h before stripping with citric acid. Recovery of surface MHC-I on the surface of LCLs was determined by flow cytometry. (G) AUC quantification of the recovery of surface MHC-I shown in F. (H) surface MHC-I levels by flow cytometry. The W6/32 antibody clone was used to detect correctly folded and assembled MHC-I molecules. (I) schematic of the Jurkat-Lucia™ NFAT detection assay. (J) Representative flow cytometry dot plot of untransduced and TCR-transduced Jurkat-Lucia™ cells. MCD19: murine CD19, was used as transduction marker. (K) recognition of peptide-pulsed LCLs by TCR-transduced Jurkat-Lucia™ cells. Cells were either left untreated or treated with torin-1 (100 nM) for 24 h before the co-culture. (L) Representative flow cytometry dot plot of untransduced and TCR-transduced primary $CD3^+$ T cells. (M) activation markers on TCR-transduced T cells after 24 h co-culture with peptide-pulsed LCLs. CD69- and 4–1BB-double-positive cells are shown as percentage of $CD3^+$ $CD8^+$ T cells. (N) IFNG/IFNγ production of $CD3^+$ TCR-transduced T cells after 24 h co-culture with peptide-pulsed LCLs. (D-H) statistical significance was determined with a two-way ANOVA, followed by multiple testing with Bonferroni correction. (K, M, N) statistical significance was determined by one-way (M, N) or two-way (K) ANOVA, followed by Tukey multiple testing. Data represents the mean ± SD of at least 3 independent experiments. (M, N) primary T cells were obtained from 4 individual healthy donors. *$p \leq 0.05$, **$p \leq 0.01$, ***$p \leq 0.001$.

CTRL and *BECN1*-KO LCL (HLA-A *2901, -A *2402, -B * 3501, -B * 4403, -C * 0401 and -C * 1601; 23 from CTRL, and 61 or 51 from two *BECN1*-KO LCLs) 66.1% (45) of all peptides were shared between the two *BECN1*-KO LCLs and 27.9% (19) were shared between CTRL and both *BECN1*-KO LCL. We next analyzed the overlaps in protein sources of the MHC-I presented peptides with the autophagosome content of CTRL and *BECN1*-KO LCLs. The respective overlap identified only three proteins (Figure S6C) but among them Calreticulin (CALR, predicted to be presented on HLA-A *2901) as one component of the PLC which was presented on MHC-I and enriched in autophagosomes of *BECN1*-KO LCLs. Furthermore, peptides of the autophagosome cargo proteins E3 ubiquitin-protein ligase RNF13 (RNF13, predicted to be presented on HLA-A *2901) and IFI30/GILT (IFI30 lysosomal thiol reductase; predicted to be presented on HLA-C * 0401) were identified as MHC-I ligands of both CRTL and *BECN1*-KO LCLs and found increased in CTRL LCL derived autophagosomes. Therefore, the MHC-I ligandomes of *BECN1*-KO and CTRL LCLs were comparable with shared sources of presented peptides. These findings further support the interpretation that in the absence of BECN1 and increased PLC incorporation into autophagosomes MHC-I assembly and transport to the cell surface is delayed, resulting in decreased $CD8^+$ T cell recognition, while MHC-I complex composition is unaltered.

DISCUSSION

This study demonstrates that while BECN1 is not essential for functional autophagy-dependent degradation in LCLs, it plays a significant role in determining autophagosomal cargo, suggesting that cargo recognition and/or recruitment represent an important aspect of its function, distinct from autophagosome formation. These findings are consistent with a previous study from Quiles *et al.* [20], which showed intact autophagosome formation in *BECN1*-deficient mouse embryonic fibroblasts and HeLa cells, despite impaired mitophagy. In our study, we did not observe a specific link between BECN1 deficiency and mitophagy, as numerous mitochondria-associated proteins were detected in autophagosomes from both, CTRL and *BECN1*-KO LCLs (Figure 4C). The absence of detectable changes in mitochondrial cargo between the two conditions is likely attributable to the use of different cellular systems. Interestingly, several other studies have found BECN1 dispensable for autophagy in a variety of cell types across different autophagy induction methods [9–18]. While some of these studies might describe non-canonical autophagy pathways, distinct from the classical starvation-induced autophagy mechanism, many could show that their mechanisms were not only dependent on the LC3 lipidation machinery, including ATG5 and ATG7 but also other core autophagy proteins such as ULK1 and PIK3C3/VPS34 [11–13,17,18,20]. In contrast, while loss of BECN1 may not impair LC3 lipidation, it has been shown to disrupt autophagy flux and lead to the formation of malformed autophagosomes in HeLa cells [19].

In this study, we demonstrate that autophagy in *BECN1*-deficient LCLs appears to be likely ULK1-dependent, as autophagy flux can be induced through starvation and MTOR inhibition (Figure 3B-D). Although autophagy is still inducible via nutrient starvation and starvation-mimicking drugs in *BECN1*-deficient LCLs, the resulting autophagic flux appears slightly reduced compared to CTRL LCLs under certain conditions, as shown by TFLC3-based assays (Figure 3C-D) and TEM (Figures 3E and 3H). This reduction may be due to an impaired autophagosome maturation and/or lysosome fusion. While it is possible that BECN1 itself serves an unknown purpose during these later stages of autophagy, previous studies have shown that the UVRAG-containing PI3K complex promotes autophagosome maturation and recruits proteins necessary for autophagosome-lysosome fusion [33,34]. Additionally, ATG14 is critically involved in autophagosome-lysosome fusion, primarily through its interaction with the STX17-SNAP29-VAMP8 complex [35,36]. Therefore, it is plausible that the reduced autophagic flux observed in *BECN1*-KO LCLs is, at least in part, a consequence of compromised ATG14 function and reduced activity of both ATG14- and UVRAG-containing PI3K complexes.

This might be counterbalanced by EBV protein expression because this virus is known to induce and utilize autophagy for its own purposes [37]. As two examples EBV latent membrane protein 1 (LMP1) induces autophagy to regulate its own autophagosomal degradation during latent infection [38]. During lytic EBV infection, autophagic membranes accumulate [39], presumably due to BFRF1 (BamH1 F fragment rightward reading frame 1)-mediated inhibition of RAB7-mediated autophosome fusion with lysosomes [40], and contribute to viral envelope acquisition during virion production [41]. These autophagic membrane accumulating functions of EBV infection might overcome attenuated autophagic flux in LCL due to absence of BECN1, but might also slow down autophagosome fusion with lysosomes.

The relationship between endosomal TLRs and autophagy remains incompletely understood. While TLR3 itself has not been identified as an autophagic cargo yet, there is evidence that its adaptor protein TRIM69/TRIF and the downstream signaling molecule TRAF6 undergo selective autophagic degradation, which can be triggered by TLR3 stimulation with poly(I:C) [27]. In this context, poly(I:C) induces autophagy via CALCOCO2-mediated recognition of TRIM69 and TRAF6, though the precise mechanism involved remains a matter of debate. In our study, we were unable to confirm autophagy induction by poly(I:C) in LCLs, which may be due to the generally low expression of TLR3 in B cells. Nevertheless, we detected TLR3 in purified autophagosomes from both CTRL and *BECN1*-KO LCLs (Figure 5A). Notably, TLR3 accumulation and increased colocalization between LC3 and TLR3 following lysosomal inhibition were only detectable in CTRL cells (Figure 5B-F). Shi *et al.* [42] demonstrated that TRIM69 directly binds to BECN1, competing with BCL2 for this interaction, with the binding increasing upon TLR3 stimulation. In BECN1-deficient cells, the absence of this interaction may reduce TRIM69 recruitment to autophagosomes. Since TLR3 has been implicated in innate immune recognition of EBV [43], BECN1 might support TLR3 targeting to autophagic degradation.

During adaptive immunity, both stably assembled MHC-I complexes as well as free MHC-I heavy chains have now been shown to be degraded via autophagy in different types of cancer [21,23] and myeloid cells [24]. In these models, active autophagy typically correlates with low levels of MHC-I surface levels which leads to reduced T cell activation. In accordance with these studies, we observed a reduction of surface MHC-I and free MHC-I heavy chain in LCLs upon autophagy activation by torin-1 (Figure 6H and S5D). Additionally, treated LCLs showed a drastically reduced MHC-I surface recovery after acid stripping (Figure 6F-G) which is probably due to an increased turnover that interferes with the trafficking of MHC-I molecules from the ER to the cell surface, delaying its replenishment on the plasma membrane. Hence, this study is the first to provide evidence for autophagy-dependent degradation of MHC-I in B cell-derived cell lines.

Interestingly, while loss of BECN1 lead to a delayed MHC-I recovery compared to CTRL LCLs in both, torin-1 treated and untreated conditions (Figure 6D-G), it did not affect MHC-I or free class I heavy chain surface levels, at least under the tested experimental conditions (Figure 6H and S5D). Furthermore, while HLA-A and -C were found as cargo in purified autophagosomes in the mass spectrometry analysis, there were no significant differences between *BECN1*-KO and CTRL LCLs detected. Based on these findings, we hypothesize that BECN1 does not play an essential role during the autophagy-dependent degradation of MHC-I molecules but rather targets ER-resident proteins that are necessary for MHC-I folding and/or peptide loading for autophagic degradation. In both of our T cell assay systems, using Jurkat-Lucia^{TM} cells as well as primary CD3$^+$ T cell from healthy donors, BECN1-deficient LCLs consistently showed an impaired ability to activate T cells (Figure 6K, M-N). As baseline surface expression of MHC-I was comparable across the different LCLs, this impairment is likely due to delayed peptide loading and/or a general high ERphagy activity in *BECN1*-KO LCLs, which results in reduced generation of stable MHC-I complexes. Notably, the *BECN1*-KO LCL C5 was consistently recognized more efficiently by both Jurkat-Lucia^{TM} and primary T cells compared to *BECN1*-KO LCL C1 (Figures 6K, 6M-N). This enhanced recognition correlates with a lower autophagic flux in C5 during starvation (Figure 3C) and slightly reduced autophagy induction following MTOR inhibition (Figure 3D), suggesting that diminished autophagy in *BECN1*-deficient cells may lead to reduced ER turnover, thereby preserving a greater pool of newly peptide loaded MHC-I complexes. Indeed more peptides could be recovered from purified MHC-I molecules of BECN1-KO LCLs but the unaltered MHC-I ligandome just argues for a delay in stable MHC-I complex assembly due to more PLC autophagy. The largely intact autophagic flux in the absence of BECN1 with more frequent targeting of the PLC seems to compromise MHC-I restricted antigen presentation and CD8$^+$ T cell recognition. These findings provide also an interesting additional explanation of BECN1 haploinsufficiency in tumor cells, such as breast and ovarian carcinoma, in which BECN1 was first described [44]. Namely, loss of BECN1 could compromise immune surveillance of these tumors by CD8$^+$ T cells.

Along these lines, the interplay between autophagy and MHC-I antigen presentation has gained significant attention and is now recognized as a key mechanism contributing to immune evasion in certain cancer types. Therefore, dissecting the precise roles of individual ATG-related proteins in MHC-I quality control, peptide loading, and surface expression is essential and will be an important focus of future research.

MATERIALS AND METHODS

Ethical statement

The cantonal ethical committee of Zurich, Switzerland, approved the use of peripheral blood samples from healthy donors (BASEC-Nr. 2019–00837).

Cell culture and drug treatments

LCLs were generated by infecting human primary B cells (HLA-B35:01$^+$) with the EBV strain B95-8 and cultured in RPMI 1640 (Gibco, 52,400–025). HEK293T cells and CD40LG/CD40L transgenic fibroblasts were cultured in Dulbecco's Modified Eagle Medium (DMEM [Gibco, 41,966–029]). Jurkat-Lucia™ NFAT reporter cells (InvivoGen, jktl-nfat) were cultured in Iscove's Modified Dulbecco's Medium (IMDM [Gibco, 21,980–032]). RPMI, DMEM and IMDM were supplemented with 10% fetal bovine serum (FBS; Merck, S0615) and 1% Pen-Strep (Thermo Fisher, 15,140,163) All cell lines were negatively tested for mycoplasma contamination regularly and kept in a humidified incubator at 37°C and 5% CO_2. Cells were treated with 100 nM torin-1 (Sigma-Aldrich, 475,991), 20 nM rapamycin (Sigma-Aldrich, R0395), 100 nM bafilomycin A_1 (Sigma-Aldrich, B1793), 50 µM chloroquine (Sigma-Aldrich, C6628), 1 µM PIK3C3/VPS34-inhibitor (compound 19; Selleckchem, S8456), 100 nM wortmannin (Selleckchem, S2758) or 25 µg/mL poly(I:C) (Merck, P1530) in full culture medium at 37°C for the indicated time periods. Starvation was performed in PBS (prepared from KCl, Na2HPO4, KH2PO4 and NaCl, Sigma-Aldrich, P3911, S3264, P0662 and 71,380) at 37°C for 24 h.

CRISPR/Cas9 crRnas design

All selected *ATG* genes were targeted with two different guide RNAs (gRNAs), aiming for the positive as well as the negative DNA strand. Predesigned gRNAs were selected from the IDT Alt-R CRISPR-Cas9 guide RNA platform, favoring high on- and off-target scores. The following gRNAs were selected:
BECN1 (+ strand): 5′-ATCTGCGAGAGACACCATCC-3′*BECN1* (- strand): 5′-GGACACGAGTTTCAAGATCC-3′*ATG4B* (+ strand): 5′-TCCTCAACGCATTCATCGAC-3′*ATG4B* (- strand): 5′-AGCAAACCGGAGAGTGTCGT-3′*ATG5* (+ strand): 5′-GGCCATCAATCGGAAACTCA-3′*ATG5* (- strand): 5′-TGATATAGCGTGAAACAAGT-3′

Generation of stable knockout LCLs

The two gRNAs were mixed with tracrRNA (IDT, 1,072,534) at equimolar concentrations and incubated at 95°C for 5 min. Cas9 (in-house) was added to the gRNA-tracrRNA duplex in a ratio of 5:1 (250 pmol duplex:50 pmol Cas9) followed by a 15-min incubation at room temperature (RT). The 3D Primary Cell 4D Nucleofector X Kit S (Lonza, V4XP-3032) was used to electroporate 5×10^5 WT LCLs in a 4D Nucleofector (Lonza) with the DN-100 pulse code. LCLs recovered in full culture medium for 2–3 days before expansion. After a sufficient recovery period (at least one week), the heterogenous LCL mixture was seeded on irradiated CD40LG transgenic fibroblasts (50 Gy) on U-bottom 96-well plates at a density of 0.9 cells per well. After 3–4 weeks, outgrowing LCLs were selected to be expanded. Knockout cell lines were confirmed by western blot and PCR/sequencing after successful expansion.

Knockout validation by sequencing

Genomic DNA was isolated from 3×10^6 LCLs using the DNeasy® Blood and Tissue Kit (QIAGEN, 69,506). The crRNA-binding regions were amplified by PCR using the Phusion™ High-Fidelity DNA Polymerase (Thermo Fisher, F530S) with the primers summarized in Table 1, followed by a PCR clean-up using the Gel and PCR clean-up kit (MACHEREY-NAGEL, 740,609.50). Sequencing was performed with the Microsynth Sanger Sequencing service, using the sequencing primers shown in Table 1. CLC Main Workbench 21 (QUIAGEN Digital Insights) was used to analyze and visualize the sequencing results.

RT-qPCR

For each condition, 3×10^6 LCLs were collected, and RNA was isolated with the RNeasy Mini kit from Qiagen (74106), following the manufacturers guidelines for cell culture samples. Reverse transcription was performed using the GoScript Reverse Transcription System from Promega (a5003). The SYBR™ Select Master Mix for CFX (Thermo Fisher, 4,472,942) was used to detect BECN1 cDNA with the following primer pairs:

F1: 5′-GCCTTTCTCCACATCCATCC-3′R1: 5′-CCATTACTTACCACAGCCCAG-3′F2: 5′-ACTCTGATTGGGGAGGCAT-3′R2: 5′-GTTTTGATGGAATAGGAGCCGC-3′

TFLC3 lentivirus production and LCL transduction

TFLC3 lentivirus was produced by $CaCl_2$ transfection in HEK293T cells. HEK293T cells were plated into 15 cm petri dishes one day prior to transfection to reach a confluency of approximately 90%. Per plate, 10 µg pMDG (Addgene, 187,440; deposited by Simon Davis, University of Oxford), 20 µg p8.91 (Addgene, 187,441; deposited by Simon Davis) and 20 µg ptfLC3 plasmid [45] were mixed in 0.25 M $CaCl_2$ in water. During thorough mixing, 1 mL 2X HEPES (2.38 g HEPES [Sigma-Aldrich, H4034], 3.28 g NaCl [Sigma-Aldrich, S3014], 80 mg Na_2HPO_4 [Sigma-Aldrich, S9390] in 200 mL H_2O, pH = 7.05) was added dropwise to the plasmid mix. After 20-min incubation at RT, the transfection mix was added to the HEK293T cells drop-by-drop. Medium was changed after 24 h. The lentivirus-containing supernatant was collected 30 h after medium change and cellular debris was removed by centrifugation for 8 min at 2000 g. The supernatant was then filtered through a 0.45 µm filter and concentrated using the PEG-it Virus Precipitation Solution (BioCat, LV825A-1), following the manufacturers protocol. LCLs were transduced in 24-well plates at a density of 5×10^5 cells per well. The lentivirus was directly added to the LCLs, followed by centrifugation for 1 h at 1500 g and 32°C. The medium was changed 24 h post transduction to increase outgrowth efficacy. GFP and RFP expression of transduced LCLs was assessed by flow cytometry using a LSRII Fortessa Cell Analyzer (BD).

TCR lentivirus production and T cell transduction

The EBV EBNA1$_{407-417}$-specific, HLA-B35:01-restricted TCR was designed based on variable regions identified by Cobo *et. al.* [31] (HPV13A10) and cloned into a pLV backbone [46,47]. TCR lentivirus was produced by PEI MAX® (Polyscience, 24,765) transfection of HEK293T cells. After seeding HEK293T in a 15-cm dish (see above), PEI MAX and plasmid DNA was mixed in serum free DMEM at a ratio of 3:2:1, corresponding to the TCR-containing plasmid, p8.91 and pMDG (Addgene, 187,441; deposited by Simon Davis; Addgene, 187,440; deposited by Simon Davis). The PEI MAX-DNA mix was incubated for 15 min at RT before adding it drop-wise to the HEK293T cells. The medium was

Table 1. PCR and sequencing primers.

Primer	Target	Purpose	Sequence (5′-3′)
BECN1_cr1_Fwd	BECN1 cr1 site	PCR	TGGAGTCCCTTCCCTGACCCTG
BECN1_cr1_Rev	BECN1 cr1 site	PCR, Sequencing	GCCCGGTCGGAAAGCTCTCAGA
BECN1_cr2_Fwd	BECN1 cr2 site	PCR	CTGTCCTCTGCCCCTGACTGCT
BECN1_cr2_Rev	BECN1 cr2 site	PCR, Sequencing	AAGGGAGAACCAGGAAAGGCCA
ATG4B_cr1_Fwd	ATG4B cr1 site	PCR, Sequencing	CCCAGCAGGGCCTCCTTCTCTT
ATG4B_cr1_Rev	ATG4B cr1 site	PCR	TGGCAGAGTTAGCAGAGAACAGT
ATG4B_cr2_Fwd	ATG4B cr2 site	PCR	CCTGGGTGAGAGAGCGAGACTC
ATG4B_cr2_Rev	ATG4B cr2 site	PCR, Sequencing	TGTGACAGCAGCGCACAGATGG
ATG5_cr1_Fwd	ATG5 cr1 site	PCR	TGCAGAATATTAGCATTGGAAGGCA
ATG5_cr1_Rev	ATG5 cr1 site	PCR, Sequencing	TGGCCTCCAAGTTCTTACAGCT
ATG5_cr2_Fwd	ATG5 cr2 site	PCR	GCGTGATCTCGGCTCACCACAA
ATG5_cr2_Rev	ATG5 cr2 site	PCWhatR, Sequencing	TGCTCCAAGTACTGACTTTGGGGT

changed 24 h later to OptiMEM (Gibco, 11,058,021). The lentivirus-containing supernatant was collected, filtered and concentrated as described above. Transduction of NFAT Jurkat-Lucia™ cells and human primary $CD3^+$ T cells was performed with 0.8 µg/mL polybrene supplementation (Sigma Aldrich, TR-1003-G). Transduction efficiency and transgenic TCR expression was assessed 4 days post transduction by flow cytometry, staining murine CD19-BV510 (Biolegend, 109,234) and the murine TCR β chain-PE (Biolegend, 152,408), respectively. Cells were acquired with a LSRII Fortessa Cell Analyzer (BD).

Western blot

Cells were resuspended in Laemmli buffer (20% PAGE 5X [20% SDS, 0.3125 M Tris-HCl in deionized water, adjusted to pH 6.8–7], 20% BBQ [50% glycerol, 20% PAGE 5X, 1% bromophenol blue in deionized water], 1.4% β-mercaptoethanol in deionized water) at a concentration of 3000 cells/µL. All samples were boiled at 95°C for 5 min before loading onto a gel. Proteins were separated by SDS-polyacrylamide gel electrophoresis (PAGE) followed by a transfer to a polyvinylidene difluoride (VWR, 10,600,023) membrane. Primary and secondary antibody incubation was performed at 4°C overnight and 1 h at RT, respectively. The following primary antibodies were used for protein detection on western blot membranes: anti-BECN1 (Santa Cruz Biotechnology, sc-48381), anti-BECN1 (proteintech, 11,306–1-AP), anti-ATG4B (Cell Signaling Technology, 5299), anti-ATG5 (Sigma-Aldrich, A0731), anti-LC3B (Novus, NB100-2220), anti-SQSTM1/p62 (1:500, American Research Products, 03-GP62-C), anti-CALCOCO2/NDP52 (invitrogen, PA5-30367), anti-SNAP29 (abcam, ab138500), anti-LC3A (Cell Signaling Technology, 4599), anti-ATG14 (proteintech, 28,021–1-AP), anti-UVRAG (Bethyl Laboratories, A301-995A), anti-GAPDH (Sigma-Aldrich, G8795), anti-VCL/vinculin (Sigma-Aldrich, V9131), anti-TLR3 (Invitrogen, MA5-16184), anti-CALR/calreticulin (invitrogen, PA3-900), anti-CANX/calnexin (Enzo, ADI-SPA-865-D), anti-TAPBP/tapasin (invitrogen, PA5102535), anti-PDIA3/ERp57 (Invitrogen, PA3009). Secondary peroxidase-conjugated antibodies were purchased from Jackson ImmunoResearch (anti-rabbit [111–035-003], anti-mouse [115–035-003], anti-guinea pig [106–035-003]). The chemiluminescence signal was developed using the WesternBright Sirius HRP kit (advansta, K-12043-D20) on a Fusion FX (Vilber Smart Imaging). Images were analyzed and quantified using ImageJ/Fiji. Quantifications were first normalized to the loading control staining (GAPDH or vinculin) and then normalized to the respective untreated control band.

Immunofluorescence staining

Cells were treated according to the experimental plan and seeded on glass coverslips in cold PBS. After a settling period of 10 min, PBS was removed carefully and cells were fixed at RT in 4% paraformaldehyde (PFA) solution (Santa Cruz Biotechnology, sc-281692) for 15 min, followed by permeabilization in 0.1% Triton X-100 (Sigma-Aldrich, T8532) for 3 min. Blocking was performed with 1% FBS for 1 h at RT. Primary and secondary antibodies were diluted in blocking solution and incubation was performed for 1 h at RT. The following primary and secondary antibodies were used: anti-LC3 (MBL, PM036), anti-SQSTM1/p62 (ARP, 03-GP62-C), anti-CALCOCO2/NDP52 (Santa Cruz Biotechnology, sc-376540), anti-TLR3 (invitrogen, MA5-16184), anti-rabbit IgG Alexa Fluor 488 (invitrogen, A11008), anti-guinea pig IgG Alexa Fluor 555 (invitrogen, A21435), anti-mouse IgG Alexa Fluor 555 (invitrogen, A21424). The cover slides were mounted on slides using DAKO fluorescent mounting medium (Agilent Technologies, S3023), supplemented with 1:2000 DAPI (Invitrogen, D1306). Images were acquired on a Leica STELLARIS 5 upright confocal laser scanning microscope using a 63x objective (NA: 1.4). Approximately 20–30 cells were imaged per condition per experiment. Every experiment was repeated three times, resulting in at least 60 data points per condition in total.

Image analysis

Representative images were visualized and processed using Fiji/ImageJ [48]. Image quantification was performed with an in-house python3.10 code. After creating composite images with ImageJ/Fiji, partial cells on the edges of the image were removed manually. After loading these composites into a python script, individual cells and intracellular foci were detected, using the scikit-image package [49]. In short, the green or red channel was used to create a binary mask of individually labeled, closed cells by considering the difference in average intensities in "cell regions" versus "non-cell regions." Then, foci were detected in the green and red channel with a user-defined intensity threshold and a size exclusion of 6 pixel (~54 µm). Foci outside cellular regions were excluded. A colocalization mask was created by combining the green and red foci mask. Then, green, red and colocalizing foci were assigned to their respective cell and the number of foci per cell was recorded. Segmentation and foci detection were visually confirmed with the napari viewer [50].

Transmission electron microscopy

For transmission electron microscopy (TEM) analysis, cells were fixed by adding an equal volume of double-strength fixative (4% formaldehyde, 5% glutaraldehyde in 0.1 M PHEM buffer (em-grade, GT140000; pH 6.9) to the culture medium for 20 min at RT. Then this fixative mixture was replaced with single-strength fixative (2% formaldehyde and 2.5% glutaraldehyde in 0.1 M PHEM buffer, pH 6.9) for 3 h at RT to further fix the cells. After 5 washes with 0.1 M PHEM buffer, pH 6.9, cells were post-fixed with 1% OsO_4 and 1% potassium ferricyanide (III) in 0.1 M PHEM buffer, pH 6.9 for 1 h on ice. After 5 washes with distilled water, cells were processed for dehydration and embedded in Epon resin (fisherscientific, 50–980-448) [51]. During the first step of dehydration, 0.5% uranyl acetate was added to the 70% ethanol solution, for post-staining, and cells were incubated at 4°C overnight. After dehydration using gradually increased concentrations of ethanol solution (90%, 96% and 100% water-

free ethanol), embedding and polymerization in Epon resin, 70-nm thin sections were cut using a Leica EM UC7 ultramicrotome (Leica Microsystems). Cell sections were collected on 50 mesh copper grids and stained with lead citrate for two min at RT as previously described [51]. Cell sections were analyzed using a 120-kV transmission electron microscope Tecnai G2 Spirit (FEI Thermo Fisher) with a digital camera (TVIPS). Quantification was performed by counting the average number of autophagosomes, degradative compartments and autolysosomes by randomly analyzing 150 cell sections per condition from three independent grids.

Autophagosome purification

After treatment with CQ (20 µM; Sigma-Aldrich, C6628) for 3 h, autophagosome purification was performed according to a published protocol [25]. In brief, a minimum of 7×10^7 cells were treated with CQ (20 µM) to increase yield and washed thoroughly with PBS before resuspending in Homogenization Medium (0.25 M sucrose [Sigma-Aldrich, S0389], 1 mM EDTA [BioForxx, 1353], 20 mM HEPES [Gibco, 15,630–056], pH 7.4 in ddH_2O). The cells were then homogenized with a Homogenizer 150 (Fisher, 15,565,809), followed by a series of centrifugation steps to enrich the vesicular fraction by removing cellular membranes and nuclei (1000 ×g for 10 min at 4°C), mitochondria (3000 ×g for 10 min at 4°C) and the cytoplasm with smaller microsomes (17000 ×g for 15 min at 4°C). The resulting vesicular pellet was then washed thoroughly with PBS again before performing a LC3B-targeted co-immunoprecipitation (see "Co-Immunoprecipitation").

Co-Immunoprecipitation

Co-IP was performed on the purified vesicular cell fraction with the Immunoprecipitation Kit Dynabeads™ Protein A (Invitrogen, 10006D) following the manufacturers guidelines. Antibodies (1–4 µg per sample) were pre-mixed with the sample before adding the Protein A Dynabeads. Anti-LC3B (Novus, NB100-2220) and rabbit isotype control IgG (invitrogen, 02–6102) were used in the co-IP assays. Washed dynabeads were snap frozen in liquid nitrogen for subsequent mass spectrometry. A non-denaturating elution was performed for analysis of the co-IP eluent by western blot, followed by lysis wih Laemmli buffer (see "Western blot").

Mass spectrometry

Mass spectrometry was performed in triplicates from snap-frozen beads after autophagosome purification. Beads were taken up with 8 M urea with 1 mM dithiothretiol in 100 mM ammonium bicarbonate (ABC) buffer pH 8.4, transferred onto 10 kDa cutoff filters (Vivacon 500, 10,000 MWCO; Sartorius, VN01H02) and spun at 10,000 g for 30 min. Proteins on the filter were alkylated with 5.5 mM IAA in 8 M urea, spun at 10'000 g for 30 min and washed twice with 100 µl of 100 mM ABC buffer. Protein digestion was performed overnight according to the FASP protocol [52]. Peptides were eluted twice with 200 µl of 100 mM ABC buffer into fresh tubes by centrifugation at 10`000 g for 30 min. Eluates were acidified with trifluoroacetic acid at a final concentration of 2% and desalted by STAGE tips prior to LC-MS /MS measurements.

LC-MS/MS measurements were performed on a QExactive HF-X mass spectrometer (Thermo Scientific) coupled to an EasyLC 1000 nanoflow-HPLC essentially as described [53]. Briefly, peptides were separated on fused silica HPLC-column tips (I.D. 75 µm, New Objective, self-packed with reprosil-Pur 120 C18-AQ, 1.9 µm [Dr. Maisch, r119.aq.] to a length of 20 cm) using a gradient of buffer A (0.1% formic acid in water) and buffer B (0.1% formic acid in 80% acetonitrile in water). The mass spectrometer was operated in data-independent mode. After each survey scan (mass range m/z = 350 – 1,200; resolution: 120,000) 28 DIA scans (isolation width of 31.4 m/z, precursors range 350–1,200 m/z) were performed. AGC target value was set to 3×10^6, resolution to 30,000 and normalized collision energy to 27%. Data were analyzed using Spectronaut software version 19 (Biognosys) with standard settings (without imputation) in directDIA mode using reference proteome of Human (UniProt, 2023, full length) and common contaminants.

Data analysis of mass spectrometry intensities was done using the Perseus 2.0.10.0 software [54]. The data was filtered for at least three valid values out of the three replicates in at least one of the experimental groups. After log2 transformation, the data was normalized to the median and missing values in the IgG negative control were imputed. Statistically significant differences between two groups were identified with a two-sided t-test using a permutation-based false-discovery rate (FDR) calculation as correction for multiple testing (250 randomizations, FDR = 0.05, S0 = 0.1). KEGG pathway analysis was on significantly enriched or reduced proteins using the STRING database [26] (grouped by similarity: ≥0.8, minimal signal shown: ≥0.01, minimal strength shown: ≥0.01, maximum FDR shown: ≤0.05).

ELISA

LCLs were seeded and treated with poly(I:C) for 24 h before collecting the supernatant. The IL27 ELISA was performed with the ELISA Flex: Human IL27 (HRP) kit from mabtech (3458–1 H), following the manufacturer's protocol. The CXCL10 ELISA was performed with the ELISA MAX™ Deluxe Set Human CXCL10 kit from Biolegend (439904) following the protocol of the manufacturer. The IFNG/IFNγ ELISA was performed with supernatant of LCLs, co-cultured with TCR-transduced primary T cells (see "Primary T cell assays"). IFNG/IFN β was measured with the ELISA Flex: human IFNG/IFN β kit from mabtech (3420–1 H-20), according to the guidelines of the manufacturer. The optical density was acquired at a Tecan Infinite 200 PRO plate reader at 450 nm, using a reference wavelength of 570 nm. A standard curve was acquired on each plate for all cytokines to determine absolute concentrations. The resulting concentrations were normalized to the respective untreated control of the measured cell line. Statistical testing was performed with a two-way ANOVA using Šidák correction for multiple testing.

Flow cytometry

LCLs were collected and stained in PBS for 30 min at 4°C with the following antibodies: anti-HLA-ABC-FITC (Biolegend, 311,404) and anti-HLA class I heavy chain (antibodies.com, A115681). Subsequent staining with a secondary anti-mouse IgG Alexa Fluor 488 antibody (invitrogen, A32723TR) was performed in combination with the anti-HLA Class I heavy chain antibody. The assays were acquired with a LSRII Fortessa Cell Analyzer (BD).

MHC-I recovery assay

Citric acid stripping of surface MHC-I molecules was adapted from a published protocol [55]. In brief, LCLs were treated accoding to the experimental outline before incubation with citric acid buffer (Thermo Fisher, J61690) (pH 3.0, supplemented with 1% FBS) for 5 min at RT. R10 was directly added to neutralize the acidic buffer and the cells were washed three times with R10. Then, stripped cells were left to rest for defined time points ranging between 1 hour to 8 h before fixation with 1% PFA. The subsequent staining was performed with an anti-HLA-ABC-FITC antibody (Biolegend, 311,404) for 30 minutes at 4°C and the assay was acquired with a LSRII Fortessa Cell Analyzer (BD).

BECN1 transcomplementation

Lentiviral vectors, encoding wild-type BECN1 or $BECN1^{R139A}$, as well as mTagBFP2, were purchased from VectorBuilder.com. Lentiviral partices were produced by $CaCl_2$ transfection of HEK293T cells followed by transduction of target LCLs (see "*TFLC3 Lentivirus production and LCL transduction*"). Successful transduction was confirmed by Flow Cytometry with a LSRII Fortessa Cell Analyzer (BD)., detecting mTagBFP2 signal and by western blot, detecting BECN1 protein expression (proteintech, 11,306–1-AP).

MHC-I internalization assay

Cells were seeded and incubated with anti-HLA-ABC-FITC (Biolegend, 311,404) for the indicated time periods in R10 at 37°C. Following incubation, cells were washed, resuspended in PBS, and allowed to settle onto glass coverslips for 10 min. Cells were then fixed with 4% PFS for 15 min. Subsequently, the plasma membrane was stained using CellBrite Blue (Biotium, 30,024) according to the manufacturer's instructions. Coverslips were mounted and imaged as decribed above (see "*Immunofluorescence staining*").

Jurkat-Lucia™ NFAT reporter assay

Jurkat-Lucia™ NFAT reporter cells were transduced with a TCR encoding lentivirus (see "TCR lentivirus production and transduction"). LCLs were peptide-pulsed overnight with 1 µM cognate EBV $EBNA1_{407–417}$ peptide (Peptide&Elephants, EP08274) and treated with autophagy inducing drugs or washed an rested for 3 h according to the experimental plan. After washing, TCR-transduced Jurkat-Lucia™ cells were added to the LCLs at a ratio of approximately 1:5. After 24 h, 20 µL of supernatant was transferred to a black 96-well plate and Lucia luciferase was detected according to the manufacturer's guidelines using Quanti-Luc 4 Reagent (InvivoGen). The luminescence signal was recorded on a Tecan Infinite 200 PRO plate reader.

Primary T cell assays

Primary $CD3^+$ T cells were isolated from healthy blood donors by PBMC isolation via density gradient centrifugation using Ficoll-Paque (GE Healthcare, 17–5442-03), followed by magnetic activated cell sorting with $CD3^+$ MicroBeads (Miltenyi, 130–050-101). Isolated $CD3^+$ T cells were activated and expanded with Dynabeads™ Human T-Activator CD3/CD28 (Gibco, 11131D) according to the manufacturer's guidelines with FCS and Pen/Strep, supplemented with 20 U/mL IL2 (PreproTech, 25–7029-42), 10 ng/mL IL7 (PreproTech, 351,336) and 1 ng/mL IL15 (PreproTech, 570,304) for 7 days. Two days after activation, Dynabeads were washed off and $CD3^+$ T cells were transduced with TCR lentivirus (see "TCR lentivirus production and T cell transduction").

LCLs were seeded and peptide-pulsed overnight with 1 µM cognate EBV $EBNA1_{407–417}$ peptide. After washing, LCLs were labeled with PKH26 (Sigma-Aldrich, MINI26-1KT) according to the protocol of the manufacturer and co-cultured with TCR-transduced primary $CD3^+$ T cells at a ratio of 1:2. Supernatant was removed after 24 h of co-culture and cells were stained with CD4-BV605 (Biolegend, 317,438), CD8-BV650 (Biolegend, 344,730), CD69-PB (Biolegend, 310,920), 4–1BB-APC (Miltenyi, 130–110-764) and Zombie-NIR (Biolegend, 423,106). The assay was acquired with a LSRII Fortessa Cell Analyzer (BD). Specific lysis of LCLs was calculated by normalizing the LCL:T cell ratio of peptide-pulsed samples to their respective non-peptide-pulsed samples.

MHC peptide isolation

MHC class I peptides were isolated by standard immunoaffinity purification using the pan-HLA class I-specific monoclonal antibody (mAb) W6/32 (produced in-house) to extract HLA-presented peptides [56].

Analysis of MHC ligands by liquid chromatography-coupled tandem mass spectrometry (LC-MS/MS)

Peptide samples were measured in five replicates by separating samples by reversed-phase liquid chromatography (nanoUHPLC, UltiMate 3000 RSLCnano, Thermo Fisher) and subsequent analysis in an online coupled Orbitrap Fusion Lumos mass spectrometer (Thermo Fisher). Peptide separation was performed at 50°C and a flow rate of 300 nL/min on a 50 µm × 25 cm separation column (PepMap C18, Thermo Fisher) applying a gradient ranging from 2.4% to 32.0% of acetonitrile (ACN) over the course of 90 min.

Eluting peptides were ionized by nanospray ionization and analyzed in the mass spectrometer by implementing top speed (3 s) data-dependent acquisition mode (DDA) followed by collision-induced dissociation (CID), generating fragment spectra with a resolution of 30,000, a mass range limited to 400–650 m/z, and positive charge states 2–3.

MHC ligand data processing

Processing was performed was performed using the computational platform Fragpipe (v21.1) including MS Fragger (v4.0), Philosopher and MSBooster and a 1% FDR for HLA class I [57–60]. HLA class I binder prediction was performed and NetMHCpan 4.1, binder threshold was set to a binder rank below 2 [61].

Statistical analysis

Statistical tests were performed with GraphPad Prism 10. Significance was tested with a one-way or two-way ANOVA using Bonferroni or Tukey correction for multiple testing, unless stated otherwise. A p-value below 0.05 was considered significant. At least three independent experiments were performed for all analyses. Analysis of a published RNA-seq dataset [30] was performed using the EMBL-EBI Single Cell Expression Atlas. Statistical significance of TEM data was evaluated using the two-tailed heteroscedastic t-test for calculating the p-values.

Disclosure statement

No potential conflict of interest was reported by the author(s).

Author contributions

CRediT: **Svenja L. Walter:** Data curation, Formal analysis, Investigation, Methodology, Project administration, Validation, Visualization, Writing – original draft, Writing – review & editing; **Felix Baur Lermer:** Data curation, Investigation, Methodology, Validation, Visualization, Writing – review & editing; **Sophie Buchser:** Data curation, Formal analysis, Investigation, Methodology, Resources, Validation, Writing – review & editing; **Sibilla Sander:** Data curation, Formal analysis, Investigation, Methodology, Resources, Validation, Writing – review & editing; **Kennith Brian Castelino:** Data curation, Formal analysis, Investigation, Methodology, Resources, Visualization, Writing – review & editing; **Marcel Wacker:** Data curation, Formal analysis, Investigation, Methodology, Validation, Visualization, Writing – review & editing; **Eanna Fennell:** Formal analysis, Software, Writing – review & editing; **Lisa Rieble:** Data curation, Investigation, Methodology, Validation, Writing – review & editing; **Saskia von Boxberg:** Data curation, Investigation, Methodology, Validation, Writing – review & editing; **Sandra Schmid:** Data curation, Investigation, Methodology, Validation, Writing – review & editing; **Christopher A. Hess:** Resources, Writing – review & editing; **Laure-Anne Ligeon:** Project administration, Supervision, Writing – review & editing; **Juliane Walz:** Funding acquisition, Project administration, Resources, Supervision, Writing – review & editing; **Muriel Mari:** Conceptualization, Project administration, Supervision, Writing – review & editing; **Fulvio Reggiori:** Conceptualization, Project administration, Supervision, Writing – review & editing; **Jörn Dengjel:** Conceptualization, Funding acquisition, Project administration, Supervision, Writing – review & editing; **Christian Münz:** Conceptualization, Funding acquisition, Project administration, Writing – original draft, Writing – review & editing.

Funding

This work was in part supported by the Swiss National Science Foundation [310030_204470/1, 310030L_197952/1 and CRSII_222718_10000065], Cancer Research Switzerland [KFS-5896–08-2023-R], the Swiss MS Society (2023–17), the Swiss State Secretariat for Education, Research and Innovation (SERI) for EU Horizon BEHIND-MS [101137235], the Sobek Foundation, the Swiss Vaccine Research Institute, Roche, Novartis and Pfizer to C.M. and the Canton and University of Fribourg as part of the SKINTEGRITY.CH research network and the Swiss National Science Foundation (grant number [316030_229588 and 310030_212187]) to J.D. The work of MW and JSW was funded by Deutsche Forschungsgemeinschaft under Germany's Excellence Strategy (Grant [EXC2180-390900677]), German Cancer Consortium (DKTK), Deutsche Forschungsgemeinschaft (DFG Grant [WA 5340/6–1]), Deutsche Krebshilfe (German Cancer Aid, [70114948], InvestBW [BW1_4064/03], Else Kröner Fresenius Foundation [EKFS 2022_EKSE.79] and Carl Zeiss Stiftung [P2024-02–012], all awarded to JSW. KBC is funded by the European Union's research and innovation programme under the Marie Skłodowska-Curie Grant Agreement No [101119795].

Data availability statement

Proteomics data will be deposited in the PRIDE repository (https://www.ebi.ac.uk/pride/).

ORCID

Muriel Mari http://orcid.org/0000-0002-2677-6945
Christian Münz http://orcid.org/0000-0001-6419-1940

References

[1] Mizushima N, Yoshimori T, Ohsumi Y. The role of Atg proteins in autophagosome formation. Annu Rev Cell Dev Biol. 2011;27(1):107–132. doi: 10.1146/annurev-cellbio-092910-154005
[2] Dooley HC, Razi M, Polson HE, et al. WIPI2 links LC3 conjugation with PI3P, autophagosome formation, and pathogen clearance by recruiting Atg12-5-16L1. Mol Cell. 2014;55(2):238–252. doi: 10.1016/j.molcel.2014.05.021
[3] Tran S, Fairlie WD, Lee EF. BECLIN1: protein structure, function and regulation. Cells. 2021;10(6):1522. doi: 10.3390/cells10061522
[4] Pattingre S, Tassa A, Qu X, et al. Bcl-2 antiapoptotic proteins inhibit beclin 1-dependent autophagy. Cell. 2005;122(6):927–939. doi: 10.1016/j.cell.2005.07.002
[5] Erlich S, Mizrachy L, Segev O, et al. Differential interactions between beclin 1 and Bcl-2 family members. Autophagy. 2007;3(6):561–568. doi: 10.4161/auto.4713
[6] Zeng X, Overmeyer JH, Maltese WA. Functional specificity of the mammalian beclin-Vps34 PI 3-kinase complex in macroautophagy versus endocytosis and lysosomal enzyme trafficking. J Cell Sci. 2006;119(2):259–270. doi: 10.1242/jcs.02735
[7] Wang RC, Wei Y, An Z, et al. Akt-mediated regulation of autophagy and tumorigenesis through beclin 1 phosphorylation. Science. 2012;338(6109):956–959. doi: 10.1126/science.1225967
[8] Wei Y, Zou Z, Becker N, et al. EGFR-mediated beclin 1 phosphorylation in autophagy suppression, tumor progression, and tumor chemoresistance. Cell. 2013;154(6):1269–1284. doi: 10.1016/j.cell.2013.08.015
[9] Scarlatti F, Maffei R, Beau I, et al. Role of non-canonical beclin 1-independent autophagy in cell death induced by resveratrol in human breast cancer cells. Cell Death Differ. 2008;15(8):1318–1329. doi: 10.1038/cdd.2008.51
[10] Zhu JH, Horbinski C, Guo F, et al. Regulation of autophagy by extracellular signal-regulated protein kinases during 1-methyl-4-phenylpyridinium-induced cell death. Am J Pathol. 2007;170(1):75–86. doi: 10.2353/ajpath.2007.060524

[11] Gao P, Bauvy C, Souquere S, et al. The Bcl-2 homology domain 3 mimetic gossypol induces both beclin 1-dependent and beclin 1-independent cytoprotective autophagy in cancer cells. J Biol Chem. 2010;285(33):25570–25581. doi: 10.1074/jbc.M110.118125

[12] Puissant A, Auberger P. AMPK- and p62/SQSTM1-dependent autophagy mediate resveratrol-induced cell death in chronic myelogenous leukemia. Autophagy. 2010;6(5):655–657. doi: 10.4161/auto.6.5.12126

[13] Smith DM, Patel S, Raffoul F, et al. Arsenic trioxide induces a beclin-1-independent autophagic pathway via modulation of SnoN/SkiL expression in ovarian carcinoma cells. Cell Death Differ. 2010;17(12):1867–1881. doi: 10.1038/cdd.2010.53

[14] Tian S, Lin J, Jun Zhou J, et al. Beclin 1-independent autophagy induced by a Bcl-XL/Bcl-2 targeting compound, Z18. Autophagy. 2010;6(8):1032–1041. doi: 10.4161/auto.6.8.13336

[15] Wong CH, Iskandar KB, Yadav SK, et al. Simultaneous induction of non-canonical autophagy and apoptosis in cancer cells by ROS-dependent ERK and JNK activation. PLOS ONE. 2010;5(4):e9996. doi: 10.1371/journal.pone.0009996

[16] Mestre MB, Fader CM, Sola C, et al. Alpha-hemolysin is required for the activation of the autophagic pathway in staphylococcus aureus-infected cells. Autophagy. 2010;6(1):110–125. doi: 10.4161/auto.6.1.10698

[17] Bhutia SK, Kegelman TP, Das SK, et al. Astrocyte elevated gene-1 induces protective autophagy. Proc Natl Acad Sci U S A. 2010;107(51):22243–22248. doi: 10.1073/pnas.1009479107

[18] Lepine S, Allegood JC, Park M, et al. Sphingosine-1-phosphate phosphohydrolase-1 regulates ER stress-induced autophagy. Cell Death Differ. 2011;18(2):350–361. doi: 10.1038/cdd.2010.104

[19] He R, Peng J, Yuan P, et al. Divergent roles of BECN1 in LC3 lipidation and autophagosomal function. Autophagy. 2015;11(5):740–747. doi: 10.1080/15548627.2015.1034404

[20] Quiles JM, Najor RH, Gonzalez E, et al. Deciphering functional roles and interplay between Beclin1 and Beclin2 in autophagosome formation and mitophagy. Sci Signal. 2023;16(770):eabo4457. doi: 10.1126/scisignal.abo4457

[21] Yamamoto K, Venida A, Yano J, et al. Autophagy promotes immune evasion of pancreatic cancer by degrading MHC-I. Nature. 2020;581(7806):100–105. doi: 10.1038/s41586-020-2229-5

[22] Berquez M, Li AL, Luy MA, et al. A multi-subunit autophagic capture complex facilitates degradation of ER stalled MHC-I in pancreatic cancer. bioRxiv. 2024. doi: 10.1101/2024.10.27.620516

[23] Herhaus L, Gestal-Mato U, Eapen VV, et al. IRGQ-mediated autophagy in MHC class I quality control promotes tumor immune evasion. Cell. 2024;187(25):7285–302 e29. doi: 10.1016/j.cell.2024.09.048

[24] Loi M, Muller A, Steinbach K, et al. Macroautophagy proteins control MHC class I levels on dendritic cells and shape anti-viral CD8$^+$ T cell responses. Cell Rep. 2016;15(5):1076–1087. doi: 10.1016/j.celrep.2016.04.002

[25] Dengjel J, Hoyer-Hansen M, Nielsen MO, et al. Identification of autophagosome-associated proteins and regulators by quantitative Proteomic analysis and genetic Screens. Mol Cell Proteomics. 2012;11(3):M111 014035. doi: 10.1074/mcp.M111.014035

[26] Szklarczyk D, Kirsch R, Koutrouli M, et al. The STRING database in 2023: protein-protein association networks and functional enrichment analyses for any sequenced genome of interest. Nucleic Acids Res. 2023;51(D1):D638–D646. doi: 10.1093/nar/gkac1000

[27] Inomata M, Niida S, Shibata K, et al. Regulation of toll-like receptor signaling by NDP52-mediated selective autophagy is normally inactivated by A20. Cell Mol Life Sci. 2012;69(6):963–979. doi: 10.1007/s00018-011-0819-y

[28] Läderach F, Piteros I, Fennell E, et al. EBV induces CNS homing of B cells attracting inflammatory T cells. Nature. 2025;646(8083):171–179. doi: 10.1038/s41586-025-09378-0

[29] SoRelle ED, Dai J, Bonglack EN, et al. Single-cell RNA-seq reveals transcriptomic heterogeneity mediated by host-pathogen dynamics in lymphoblastoid cell lines. Elife. 2021;10. doi: 10.7554/eLife.62586

[30] Mrozek-Gorska P, Buschle A, Pich D, et al. Epstein-Barr virus reprograms human B lymphocytes immediately in the prelatent phase of infection. Proc Natl Acad Sci U S A. 2019;116(32):16046–16055. doi: 10.1073/pnas.1901314116

[31] Lammoglia Cobo MF, Welters C, Rosenberger L, et al. Rapid single-cell identification of Epstein-Barr virus-specific T-cell receptors for cellular therapy. Cytotherapy. 2022;24(8):818–826. doi: 10.1016/j.jcyt.2022.03.005

[32] Heberle H, Meirelles GV, da Silva FR, et al. InteractiVenn: a web-based tool for the analysis of sets through venn diagrams. BMC Bioinf. 2015;16(1):169. doi: 10.1186/s12859-015-0611-3

[33] Matsunaga K, Saitoh T, Tabata K, et al. Two beclin 1-binding proteins, Atg14L and Rubicon, reciprocally regulate autophagy at different stages. Nat Cell Biol. 2009;11(4):385–396. doi: 10.1038/ncb1846

[34] Liang XH, Kleeman LK, Jiang HH, et al. Protection against fatal sindbis virus encephalitis by beclin, a novel Bcl-2-interacting protein. J Virol. 1998;72(11):8586–8596. doi: 10.1128/JVI.72.11.8586-8596.1998

[35] Diao J, Liu R, Rong Y, et al. ATG14 promotes membrane tethering and fusion of autophagosomes to endolysosomes. Nature. 2015;520(7548):563–566. doi: 10.1038/nature14147

[36] Liu R, Zhi X, Zhong Q. ATG14 controls SNARE-mediated autophagosome fusion with a lysosome. Autophagy. 2015;11(5):847–849. doi: 10.1080/15548627.2015.1037549

[37] Münz C, Campbell GR, Esclatine A, et al. Autophagy machinery as exploited by viruses. Autophagy Rep. 2025;4(1):2464986. doi: 10.1080/27694127.2025.2464986

[38] Lee DY, Sugden B. The latent membrane protein 1 oncogene modifies B-cell physiology by regulating autophagy. Oncogene. 2008;27(20):2833–2842. doi: 10.1038/sj.onc.1210946

[39] Nowag H, Guhl B, Thriene K, et al. Macroautopphagy proteins assist Epstein Barr virus production and get incorporated into the virus particles. EBioMedicine. 2014;1(2–3):116–125. doi: 10.1016/j.ebiom.2014.11.007

[40] Gonnella R, Dimarco M, Farina GA, et al. BFRF1 protein is involved in EBV-mediated autophagy manipulation. Microbes Infect. 2020;22(10):585–591. doi: 10.1016/j.micinf.2020.08.002

[41] Pena-Francesch M, Vanoaica LD, Zhu GF, et al. The autophagy machinery interacts with EBV capsids during viral envelope release. Proc Natl Acad Sci U S A. 2023;120(34):e2211281120. doi: 10.1073/pnas.2211281120

[42] Shi CS, Kehrl JH. MyD88 and trif target Beclin 1 to trigger autophagy in macrophages. J Biol Chem. 2008;283(48):33175–33182. doi: 10.1074/jbc.M804478200

[43] Iwakiri D, Zhou L, Samanta M, et al. Epstein-Barr virus (EBV)-encoded small RNA is released from EBV-infected cells and activates signaling from toll-like receptor 3. J Exp Med. 2009;206(10):2091–2099. doi: 10.1084/jem.20081761

[44] Liang XH, Jackson S, Seaman M, et al. Induction of autophagy and inhibition of tumorigenesis by beclin 1. Nature. 1999;402(6762):672–676. doi: 10.1038/45257

[45] Kimura S, Noda T, Yoshimori T. Dissection of the autophagosome maturation process by a novel reporter protein, tandem fluorescent-tagged LC3. Autophagy. 2007;3(5):452–460. doi: 10.4161/auto.4451

[46] Thomas S, Mohammed F, Reijmers RM, et al. Framework engineering to produce dominant T cell receptors with enhanced antigen-specific function. Nat Commun. 2019;10(1):4451. doi: 10.1038/s41467-019-12441-w

[47] Böni M, Peng S, Vanoaica D, et al. LANA-Specific CD4$^+$ effector T cells accumulate at the site of KSHV infection in humanized mice. Nat Commun. 2025;17(1):282. doi: 10.1038/s41467-025-66992-2

[48] Schindelin J, Arganda-Carreras I, Frise E, et al. Fiji: an open-source platform for biological-image analysis. Nat Methods. 2012;9(7):676–682. doi: 10.1038/nmeth.2019

[49] van der Walt S, Schonberger JL, Nunez-Iglesias J, et al. Scikit-image: image processing in Python. PeerJ. 2014;2:e453. doi: 10.7717/peerj.453

[50] Chiu C-L, Clack N. Napari: a python multi-dimensional image viewer platform for the Research community. Microscopy Microanal. 2022;28(S1):1576–1577. doi: 10.1017/S1431927622006328

[51] Verheije MH, Raaben M, Mari M, et al. Mouse hepatitis coronavirus RNA replication depends on GBF1-mediated ARF1 activation. PLoS Pathog. 2008;4(6):e1000088. doi: 10.1371/journal.ppat.1000088

[52] Wisniewski JR, Zougman A, Nagaraj N, et al. Universal sample preparation method for proteome analysis. Nat Methods. 2009;6(5):359–362. doi: 10.1038/nmeth.1322

[53] Sankar DS, Kaeser-Pebernard S, Vionnet C, et al. The ULK1 effector BAG2 regulates autophagy initiation by modulating AMBRA1 localization. Cell Rep. 2024;43(9):114689. doi: 10.1016/j.celrep.2024.114689

[54] Yu SH, Ferretti D, Schessner JP, et al. Expanding the Perseus software for Omics data analysis with custom Plugins. Curr Protoc Bioinf. 2020;71(1):e105. doi: 10.1002/cpbi.105

[55] Sugawara S, Abo T, Kumagai K. A simple method to eliminate the antigenicity of surface class I MHC molecules from the membrane of viable cells by acid treatment at pH 3. J Immunol Methods. 1987;100(1–2):83–90. doi: 10.1016/0022-1759(87)90175-x

[56] Nelde A, Kowalewski DJ, Stevanovic S. Purification and identification of naturally presented MHC class I and II ligands. Methods Mol Biol. 2019;1988:123–136. doi: 10.1007/978-1-4939-9450-2_10

[57] da Veiga Leprevost F, Haynes SE, Avtonomov DM, et al. Philosopher: a versatile toolkit for shotgun proteomics data analysis. Nat Methods. 2020;17(9):869–870. doi: 10.1038/s41592-020-0912-y

[58] Kong AT, Leprevost FV, Avtonomov DM, et al. Msfragger: ultrafast and comprehensive peptide identification in mass spectrometry-based proteomics. Nat Methods. 2017;14(5):513–520. doi: 10.1038/nmeth.4256

[59] Yang KL, Yu F, Teo GC, et al. Msbooster: improving peptide identification rates using deep learning-based features. Nat Commun. 2023;14(1):4539. doi: 10.1038/s41467-023-40129-9

[60] Yu F, Haynes SE, Teo GC, et al. Fast quantitative analysis of timsTOF PASEF data with MSFragger and IonQuant. Mol Cell Proteomics. 2020;19(9):1575–1585. doi: 10.1074/mcp.TIR120.002048

[61] Reynisson B, Alvarez B, Paul S, et al. NetMHCpan-4.1 and NetMHCIIpan-4.0: improved predictions of MHC antigen presentation by concurrent motif deconvolution and integration of MS MHC eluted ligand data. Nucleic Acids Res. 2020;48(W1):W449–W454. doi: 10.1093/nar/gkaa379